PERTURBED DYNAMIC TIME WARPING: A PROBABILISTIC FRAMEWORK AND GENERALIZED VARIANTS

Xiangqian Sun[*1], **Chaoqun Wang**[2], **Wei Zhang**[3]
[1]School of Mathematics and Physics, Xi'an Jiaotong-Liverpool University, China
[2]School of AI and Advanced Computing, Xi'an Jiaotong-Liverpool University, China
[3]School of Management, Zhejiang University, China
{Xiangqian.Sun, Chaoqun.Wang}@xjtlu.edu.cn, wei_zhang@zju.edu.cn

ABSTRACT

Dynamic Time Warping (DTW) is a classical method for measuring similarity between time series, but its non-differentiability hinders integration into end-to-end learning frameworks. To address this, soft-DTW replaces the minimum operator with a smooth soft-min, enabling differentiability and efficient computation. Motivated by soft-DTW, we propose perturbed-DTW, a differentiable framework of DTW obtained by adding random perturbations to warping costs and taking the expected minimum. Under Gumbel noise, perturbed-DTW exactly recovers soft-DTW, providing a natural probabilistic interpretation of soft-DTW. We further generalize this framework by extending the Gumbel noise to the broader family of generalized extreme value (GEV) distributions, leading to a new class of soft-DTW variants. Building on this insight, we introduce nested-soft-DTW (ns-DTW), which integrates GEV perturbations into the dynamic programming formulation of perturbed-DTW. This extension induces alignments with tunable skewness, offering greater flexibility in modeling diverse alignment structures. We validate ns-DTW on barycenter computation, clustering, and classification, demonstrating its effectiveness over existing approaches.

1 INTRODUCTION

Dynamic Time Warping (DTW) is a classical measure of similarity between time series that computes the minimum-cost alignment between two sequences (Berndt & Clifford, 1994; Sakoe & Chiba, 2003). Unlike Euclidean distance, DTW accommodates temporal distortions and unequal sequence lengths, making it broadly applicable across domains such as object recognition (Belongie et al., 2002), time-series forecasting (Le Guen & Thome, 2019), and irregular sequence modeling (Zhang et al., 2023). Despite its effectiveness, DTW is limited by the non-differentiable nature of its minimum operator, rendering it incompatible with gradient-based optimization methods.

To address non-differentiability, Cuturi & Blondel (2017) introduced *soft-DTW*, which replaces the hard minimum with a smooth soft-min operator. Soft-DTW admits efficient dynamic programming and yields gradients that can be computed recursively. Thereby, it enables gradient-based optimization in applications such as music score alignment (Mensch & Blondel, 2018), video segmentation (Chang et al., 2019) and trajectory clustering (Brankovic et al., 2020).

Motivated by soft-DTW, we extend the differentiable DTW framework through the lens of *perturbed optimizer* (Berthet et al., 2020). We propose **perturbed-DTW**, a new scheme that introduces randomness into the alignment costs, computes the minimum perturbed cost, and then averages over the noise distribution. This formulation naturally yields a differentiable relaxation: the optimal alignment matrix becomes a distribution over paths rather than a single deterministic solution. Interestingly, when the perturbations are Gumbel distributed, perturbed-DTW recovers soft-DTW. This provides a new probabilistic interpretation of soft-DTW as the expectation of DTW under Gumbel perturbations.

[*]corresponding author

Building on perturbed-DTW, we introduce **nested-soft-DTW (ns-DTW)**, a novel variant obtained by employing the generalized extreme value (GEV) distribution as the perturbation. By modeling correlations across groups of variables, ns-DTW captures richer alignment structures. Remarkably, the resulting alignments of ns-DTW can exhibit tunable skewness beyond what soft-DTW allows.

Our contributions are threefold:

- We introduce perturbed-DTW, a general perturbation-based framework for differentiable DTW. Within this framework, soft-DTW emerges naturally as the expectation of DTW when alignment costs are perturbed by Gumbel noise, thereby providing a probabilistic interpretation of its smoothing behavior.
- By adopting GEV perturbations, we derive ns-DTW, which offers greater modeling flexibility through correlated perturbations and skewed alignment distributions.
- We demonstrate the effectiveness of ns-DTW on diverse time-series tasks, showing that it captures meaningful alignment structures while remaining computationally tractable.

The remainder of the paper is organized as follows. Section 2 reviews DTW and soft-DTW. Section 3 presents perturbed-DTW and its connection to soft-DTW, and introduces ns-DTW and its properties. Section 4 provides experimental results across benchmark datasets.

2 Preliminaries

2.1 Dynamic Time Warping

Consider two p-dimensional time series $\mathbf{x} = [\boldsymbol{x}_1, \ldots, \boldsymbol{x}_m] \in \mathbb{R}^{p\times m}$ and $\mathbf{y} = [\boldsymbol{y}_1, \ldots, \boldsymbol{y}_n] \in \mathbb{R}^{p\times n}$. Denote $[m] = \{1, \ldots, m\}$ and $[n] = \{1, \ldots, n\}$. *Dynamic time warping* (DTW) aims to find the optimal alignment between two sequences by allowing a point in one sequence to be matched with one or more points in the other. To formulate the optimal alignment problem, we first define the alignment cost. A *local cost matrix* $\boldsymbol{C} \in \mathbb{R}^{m\times n}$ measures element-wise dissimilarities: $[\boldsymbol{C}(\mathbf{x}, \mathbf{y})]_{i,j} = c(\boldsymbol{x}_i, \boldsymbol{y}_j)$, where $c(\cdot,\cdot) : \mathbb{R}^p \times \mathbb{R}^p \to \mathbb{R}_+$ is a differentiable cost function. A commonly used cost function adopts the squared Euclidean distance, that is,

$$[\boldsymbol{C}(\mathbf{x}, \mathbf{y})]_{i,j} = c(\boldsymbol{x}_i, \boldsymbol{y}_j) = \frac{1}{2}\|\boldsymbol{x}_i - \boldsymbol{y}_j\|_2^2, \quad \forall i \in [m],\ j \in [n].$$

Then, an *alignment matrix* $\boldsymbol{A} \in \{0, 1\}^{m\times n}$ encodes an alignment between data points $\boldsymbol{x}_i$ and $\boldsymbol{y}_j$: $A_{i,j} = 1$ if $\boldsymbol{x}_i$ is aligned with $\boldsymbol{y}_j$, and 0 otherwise. In addition, we call a alignment matrix is *valid* if it satisfies: (i) the nonzero entries of $\boldsymbol{A}$ form a path starting from $(1, 1)$ and ending at (m, n); (ii) the moves in the path can only be one of the directions: $\{\rightarrow, \downarrow, \searrow\}$. Denote the set of *all valid alignment matrices* as $\mathcal{A}_{m,n}$. Given the local cost matrix $\boldsymbol{C}$ and the alignment matrix $\boldsymbol{A} \in \mathcal{A}_{m,n}$, DTW is defined as

$$\mathrm{DTW}(\boldsymbol{C}) \coloneqq \min_{\boldsymbol{A}\in\mathcal{A}_{m,n}} \langle \boldsymbol{A}, \boldsymbol{C}\rangle, \tag{1}$$

where $\langle \boldsymbol{A}, \boldsymbol{C}\rangle = \mathrm{Trace}(\boldsymbol{C}^\top \boldsymbol{A})$ is the sum of elementwise products (Frobenius inner product). *Optimal alignment matrix* $\boldsymbol{A}^*$ is defined as the one that achieves the minimum cost

$$\boldsymbol{A}^* = \operatorname*{arg\,min}_{\boldsymbol{A}\in\mathcal{A}_{m,n}} \langle \boldsymbol{A}, \boldsymbol{C}\rangle. \tag{2}$$

However, directly computing DTW via (1) is intractable due to the exponential size of $\mathcal{A}_{m,n}$. Instead, DTW can be computed efficiently via dynamic programming (DP). To formulate the DP, define $D_{i,j}$ as the minimal cost of alignment from time series $[\boldsymbol{x}_1, \ldots, \boldsymbol{x}_i]$ and $[\boldsymbol{y}_1, \ldots, \boldsymbol{y}_j]$. Then, $D_{i,j}$ satisfies the Bellman equation (Bellman, 1952),

$$D_{i,j} = \min\{\underbrace{D_{i,j-1}}_{A_{i,j-1}=1}, \underbrace{D_{i-1,j}}_{A_{i-1,j}=1}, \underbrace{D_{i-1,j-1}}_{A_{i-1,j-1}=1}\} + C_{i,j}\,, \quad \forall 1 < i \le m, 1 < j \le n. \tag{3}$$

with boundary conditions $D_{i,1} = \sum_{k=1}^{i} C_{k,1}$, $\forall i \in [m]$, and $D_{1,j} = \sum_{k=1}^{j} C_{1,k}$, $\forall j \in [n]$. Then DTW distance is then given by $D_{m,n}$, i.e., $\mathrm{DTW}(\boldsymbol{C}) = D_{m,n}$. Therefore, the optimal alignment path can be recovered by backtracking from $D_{m,n}$ to $D_{1,1}$ from (3). This approach guarantees that the optimal solution is found by considering all possible alignment paths while avoiding the exponential complexity of exhaustive enumeration.

Equation (3) enables efficient computation of both the DTW distance and its optimal alignment via dynamic programming. Yet, the inherent non-differentiability of DTW, stemming from the minimum operator, precludes its use in end-to-end learning pipelines. Introducing differentiability without sacrificing computational efficiency is a central challenge in extending DTW to modern learning frameworks (Cuturi & Blondel, 2017).

2.2 SOFT-DTW

Cuturi & Blondel (2017) proposed *soft-DTW*, a differentiable relaxation of DTW that replaces the minimum operator in Equation (1) with a smooth approximation (Cuturi et al., 2007; Saigo et al., 2006) . Technically, for a vector $\boldsymbol{x} = (x_1, \ldots, x_n)$, the *soft minimum* operator is defined as

$$\min\nolimits_\gamma \boldsymbol{x} = -\gamma \log \sum_{i=1}^{n} \exp(-\frac{x_i}{\gamma}) \ ,$$

where $\gamma > 0$ is the *temperature parameter* to control the smoothness and bias. In particular, $\min_\gamma \boldsymbol{x}$ approaches $\min \boldsymbol{x}$ as $\gamma \to 0$ while it approaches $-\gamma \log n$ as $\gamma \to \infty$. Formally, soft-DTW is defined as

$$\text{soft-DTW}_\gamma(\boldsymbol{C}) := \min\nolimits_\gamma \langle \mathbf{A}, \mathbf{C} \rangle = -\gamma \log \sum_{\boldsymbol{A} \in \mathcal{A}_{m,n}} \exp\left(-\frac{\langle \boldsymbol{A}, \boldsymbol{C} \rangle}{\gamma}\right), \tag{4}$$

where $\langle \mathbf{A}, \mathbf{C} \rangle := \big(\langle \boldsymbol{A}, \boldsymbol{C} \rangle\big)_{\boldsymbol{A} \in \mathcal{A}_{m,n}} \in \mathbb{R}^{|\mathcal{A}_{m,n}|}$ denotes the vector whose entries are the alignment costs $\langle \boldsymbol{A}, \boldsymbol{C} \rangle$ concatenated over all alignments in $\mathcal{A}_{m,n}$. The soft-minimum operator here maps vector of all possible alignment costs into an "aggregated" cost. Noted that soft-DTW is a differentiable discrepancy compared to DTW, and it converges to DTW when $\gamma \to 0$. Conversely, as $\gamma \to \infty$, soft-DTW approaches the mean of all possible alignment costs.

The differentiability of soft-DTW with respect to both the time series $\mathbf{x}$, $\mathbf{y}$ and the cost matrix $\boldsymbol{C}$ enables its use in gradient-based learning algorithms. This property makes it particularly valuable for applications in machine learning and optimization. Notably, the optimal alignment matrix in soft-DTW is no longer deterministic; instead, it follows a Gibbs distribution over $\mathcal{A}_{m,n}$:

$$P(\boldsymbol{A}; \boldsymbol{C}) = \frac{\exp\big(-\langle \boldsymbol{A}, \boldsymbol{C} \rangle / \gamma\big)}{\sum_{\boldsymbol{A}' \in \mathcal{A}_{m,n}} \exp\big(-\langle \boldsymbol{A}', \boldsymbol{C} \rangle / \gamma\big)}. \tag{5}$$

The expected alignment matrix is

$$\boldsymbol{E} = \sum_{A \in \mathcal{A}_{m,n}} P(\boldsymbol{A}; \boldsymbol{C}) \cdot \boldsymbol{A}.$$

Here, $E_{i,j} \in (0, 1)$ represents the marginal probability that $\boldsymbol{x}_i$ is aligned with $\boldsymbol{y}_j$. Although soft-DTW has a succinct form, direct evaluating (4) is computationally challenging, as it requires summing over all possible alignment matrices. However, Mensch & Blondel (2018) showed that soft-DTW can be reformulated as entropy-regularized dynamic programming. Specifically, one can obtain the *soft accumulated cost matrix* $\boldsymbol{S}$ by replacing the hard minimum in the DTW recursion (3) with the soft minimum:

$$S_{i,j} = \min\nolimits_\gamma \left\{ S_{i-1,j-1},\ S_{i-1,j},\ S_{i,j-1} \right\} + C_{i,j}.$$

This recursion yields $\text{soft-DTW}_\gamma(\boldsymbol{C}) = S_{m,n}$ (Cuturi & Blondel, 2017). Additionally, soft-DTW admits an alternative variational formulation, expressed as the solution to an entropy-regularized linear program (Blondel et al., 2021). Let

$$\boldsymbol{p}(\boldsymbol{C}) := \big(P(\boldsymbol{A}; \boldsymbol{C})\big)_{\boldsymbol{A} \in \mathcal{A}_{m,n}} \in \Delta^{|\mathcal{A}_{m,n}|} \quad \text{and} \quad \boldsymbol{s}(\boldsymbol{C}) := \langle \mathbf{A}, \mathbf{C} \rangle \in \mathbb{R}^{|\mathcal{A}(m,n)|}.$$

denote the vector of alignment matrix probabilities and its corresponding alignment costs, respectively.[1] Thus, soft-DTW can be expressed in the variational form:

$$\text{soft-DTW}_\gamma = \min_{\boldsymbol{p}\in\Delta^{|\mathcal{A}_{m,n}|}} \langle \boldsymbol{p}, \boldsymbol{s}\rangle + \gamma H(\boldsymbol{p}), \tag{6}$$

where $H(\boldsymbol{p}) = \langle \boldsymbol{p}, \log \boldsymbol{p}\rangle$ denotes the negative Shannon entropy. This variational perspective highlights soft-DTW as an entropy-regularized alignment cost (Blondel et al., 2020; Sun et al., 2023), as illustrated in Figure 1

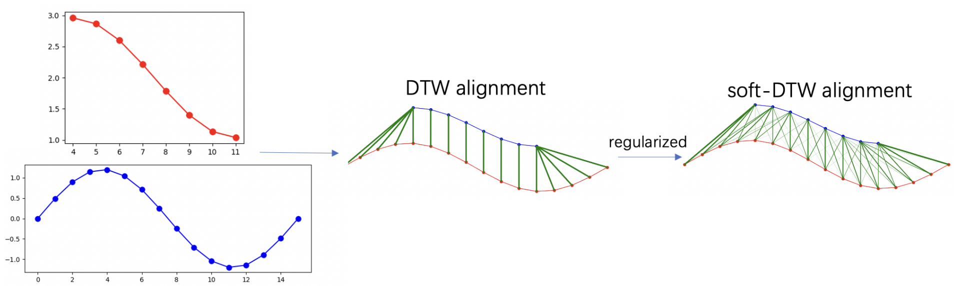

Figure 1: An illustration of soft-DTW. The right one is the expected alignment of soft-DTW.

3 Perturbed Dynamic Time Warping

3.1 Perturbed-DTW Definition

In this section, we introduce perturbed-DTW, a new scheme that provides an alternative means of rendering the original DTW differentiable. Let $\boldsymbol{x} = (x_1, \ldots, x_n)^\top \in \mathbb{R}^n$ and let $\boldsymbol{\varepsilon} = (\varepsilon_1, \ldots, \varepsilon_n)^\top$ denote a perturbation vector drawn from a distribution $\mathbb{P}$. For temperature parameter $\gamma > 0$, define the perturbed minimum as

$$\mathbb{E}_{\boldsymbol{\varepsilon}\sim\mathbb{P}}\big[\min\{\boldsymbol{x} - \gamma\boldsymbol{\varepsilon}\}\big] = \mathbb{E}_{\boldsymbol{\varepsilon}\sim\mathbb{P}}\big[\min\{x_1 - \gamma\varepsilon_1, \cdots, x_n - \gamma\varepsilon_n\}\big]. \tag{7}$$

Next, we define the perturbed-DTW by replacing the standard minimum operator in the DTW with this perturbed version.

Definition 1. *The perturbed-DTW is defined as*

$$\text{perturbed-DTW}_\gamma(C) := \mathbb{E}_{\boldsymbol{\varepsilon}\sim\mathbb{P}}\left[\min\left\{\langle \mathbf{A}, \mathbf{C}\rangle - \gamma\boldsymbol{\varepsilon}\right\}\right] \tag{8}$$

where $\boldsymbol{\varepsilon}$ is a perturbation vector of dimension $|\mathcal{A}_{m,n}|$ distributed according to $\mathbb{P}$, and $\gamma > 0$ is the temperature parameter.

Intuitively, our method first perturbs the cost of each valid alignment with a random noise term $\gamma\varepsilon$, and then takes the minimum over all possible alignment matrices. The final result is the expectation of this minimum value with respect to the probability distribution of the noise. The expected alignment under perturbed-DTW can be treated as an aggregated version of DTW alignments under different realizations of ε, as shown in Figure 2 . This formulation is closely related to **random utility theory** (Train, 2009) , where choices are made based on utilities perturbed by random shocks. Unlike soft-DTW, which relies on a heuristic soft-minimum operator, perturbed-DTW achieves differentiability through randomization. This approach establishes a deep connection between time series alignment and random utility models, where an alignment matrix A represents a choice with a utility of $-\langle \boldsymbol{A}, \boldsymbol{C}\rangle$, and $\gamma\boldsymbol{\varepsilon}$ acts as a random utility shock.

Example: Gumbel Perturbation. We consider the i.i.d. Gumbel distribution for the perturbation noise and this choice recovers the soft-DTW. Our result is based on the following lemma.

[1]For notational simplicity, we omit the explicit dependence on $\boldsymbol{C}$ and write $\boldsymbol{p}$ and $\boldsymbol{s}$.

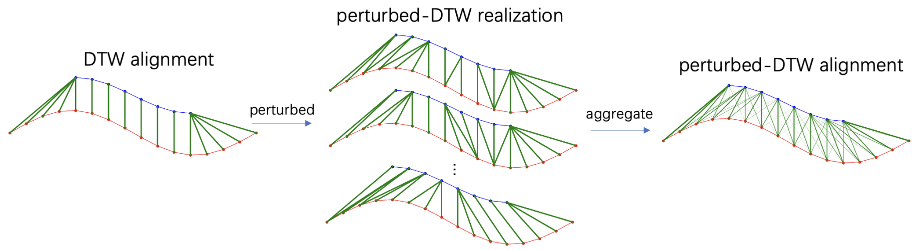

Figure 2: An illustration of perturbed-DTW. The left one is the alignment under the DTW, the middle one is the alignments under different random noise realizations, and the right one can be treated as the aggregation of middle ones and it is also the alignment under soft-DTW.

Lemma 1. *If ε are i.i.d. Gumbel$(-c, 1)$ distributed, where $c \approx 0.5772$ is the Euler-Mascheroni constant, then*

$$\mathbb{E}\Big[\min\{x_1 - \gamma\varepsilon_1, \ldots, x_n - \gamma\varepsilon_n\}\Big] = -\gamma \log \sum_{i=1}^{n} \exp(-\frac{x_i}{\gamma}), \tag{9}$$

This lemma leverages the property of Gumbel distribution, since the minimum of Gumbel variables corresponds to the negative maximum of their negations. Based on this lemma, we can obtain the following result which induces soft-DTW.

Proposition 1. *The perturbed-DTW under i.i.d. Gumbel$(-c, 1)$ perturbation is*

$$\text{perturbed-DTW}_\gamma(\boldsymbol{C}) \coloneqq \mathbb{E}\left[\min\left\{\langle \mathbf{A}, \mathbf{C}\rangle - \gamma\boldsymbol{\varepsilon}\right\}\right] = -\gamma \log \sum_{\boldsymbol{A}\in\mathcal{A}_{m,n}} \exp\left(-\frac{\langle \boldsymbol{A}, \boldsymbol{C}\rangle}{\gamma}\right).$$

In addition, the optimal alignment matrix in perturbed-DTW is

$$P(\boldsymbol{A}; \boldsymbol{C}) = \mathbb{E}\left[\arg\min_{\boldsymbol{A}}\left\{\langle \mathbf{A}, \mathbf{C}\rangle - \gamma\boldsymbol{\varepsilon}\right\}\right] = \frac{\exp\big(-\langle \boldsymbol{A}, \boldsymbol{C}\rangle/\gamma\big)}{\sum_{\boldsymbol{A}'\in\mathcal{A}_{m,n}} \exp\big(-\langle \boldsymbol{A}', \boldsymbol{C}\rangle/\gamma\big)}.$$

Example : Generalized Extreme Value Perturbation. Beyond the Gumbel case, other perturbation families yield new differentiable relaxations. In particular, we extend the perturbation framework by modeling the random noise with the generalized extreme value (GEV) distribution. Before proceeding, we briefly recall the definition of the GEV distribution.

To formalize this setting, we partition $\mathcal{A}_{m,n}$ into J groups, with the j-th group containing K_j elements, such that $\sum_{j=1}^{J} K_j = |\mathcal{A}_{m,n}|$. We index groups by j and denote by k the alignment matrix associated with the k-th element of group j. Then, the cumulative distribution function (CDF) of GEV joint distribution is

$$F(\varepsilon_{11}, \ldots, \varepsilon_{JK_J}) = \exp\left(-\sum_{j=1}^{J}\left[\sum_{k=1}^{K_j} \exp\left(-\frac{\varepsilon_{jk}}{\tau_j}\right)\right]^{\tau_j}\right). \tag{10}$$

where $0 < \tau_\ell \leq 1$ is the similarity parameter. Intuitively, the GEV distribution can be regarded as a correlated multivariate generalization of the Gumbel distribution. By adopting the GEV perturbation, we obtain the following result and denote the new variant as *nested-soft-DTW*, dubbed ns-DTW$_\gamma(\boldsymbol{C})$.

Theorem 1. *If the GEV errors are centered to have mean zero (i.e. $\tilde{\varepsilon}_{jk} = \varepsilon_{jk} - c$), the perturbed-DTW under $\tilde{\boldsymbol{\varepsilon}}$ has the following expression:*

$$\text{ns-DTW}_\gamma(\boldsymbol{C}) \coloneqq \mathbb{E}\left[\min\left\{\langle \mathbf{A}, \mathbf{C}\rangle - \gamma\tilde{\boldsymbol{\varepsilon}}\right\}\right] = -\gamma \log\left(\sum_{\ell=1}^{J}\left(\sum_{A\in\ell} \exp\left(-\frac{\langle \boldsymbol{A}, \boldsymbol{C}\rangle}{\gamma\tau_\ell}\right)\right)^{\tau_\ell}\right) \tag{11}$$

Moreover, if A is the kth one in group j, the corresponding probability is

$$P(\boldsymbol{A}; \boldsymbol{C}) = \frac{\left(\sum_{\boldsymbol{A}'\in j} \exp\left(-\frac{\langle \boldsymbol{A}', \boldsymbol{C}\rangle}{\gamma\tau_j}\right)\right)^{\tau_j - 1}}{\sum_{\ell=1}^{J}\left(\sum_{\boldsymbol{A}'\in\ell} \exp\left(-\frac{\langle \boldsymbol{A}', \boldsymbol{C}\rangle}{\gamma\tau_\ell}\right)\right)^{\tau_\ell}} \cdot \exp\left(-\frac{\langle \boldsymbol{A}, \boldsymbol{C}\rangle}{\gamma\tau_j}\right)$$

The idea of GEV can also be found in the nest logit model from random utility theory (Train, 2009). Note that perturbed-DTW under GEV perturbation presents groupwise correlation between different $\boldsymbol{A}$ when $0 < \tau_\ell < 1$ and it reduces to soft-DTW when $\tau_\ell = 1, \forall \ell$. Additionally, we can also write it into a variational form.

Proposition 2. *The perturbed-DTW under GEV perturbation in Equation (11) can be written into variational form:*

$$\text{ns-DTW}_\gamma(\boldsymbol{C}) = \min_{\boldsymbol{p} \in \Delta^{|\mathcal{A}(m,n)|}} \langle \boldsymbol{p}, \boldsymbol{s} \rangle + \gamma H(\boldsymbol{p}), \tag{12}$$

where

$$H(\boldsymbol{p}) = \sum_{\ell=1}^{J} \sum_{m=1}^{K_\ell} \tau_\ell p_{\ell m} \log p_{\ell m} - \sum_{\ell=1}^{J} (\tau_\ell - 1) \left(\sum_{m=1}^{K_\ell} p_{\ell m} \right) \log \left(\sum_{m=1}^{K_\ell} p_{\ell m} \right). \tag{13}$$

We call the regularization term (13) as *nested Shannon entropy* (Fosgerau et al., 2020) and it reduce to Shannon entropy when $\tau_\ell = 1, \forall \ell$. The following proposition characterizes some properties of perturbed-DTW.

Proposition 3 (Properties of perturbed-DTW)**.** *The following properties hold for perturbed-DTW:*

1. *(Scaling)* $\text{perturbed-DTW}_\gamma(\boldsymbol{C}) = \gamma \, \text{perturbed-DTW}_1(\boldsymbol{C}/\gamma)$.
2. *(Optimal Alignment matrix distribution) The distribution of the alignment matrix is given by* $P(\boldsymbol{A}; \boldsymbol{C}) = \mathbb{E}\left[\arg\min_{\boldsymbol{A}} \left\{ \langle \mathbf{A}, \mathbf{C} \rangle - \gamma \boldsymbol{\varepsilon} \right\}\right]$.
3. *(Gradient) The gradient of perturbed-DTW with respect to C is expected alignment matrix* $\boldsymbol{E} = \sum_{\boldsymbol{A} \in \mathcal{A}_{m,n}} \boldsymbol{A} \cdot P(\boldsymbol{A}; \boldsymbol{C})$.
4. *(Asymptotic)* $\text{perturbed-DTW}_\gamma(\boldsymbol{C}) \to \text{DTW}(\boldsymbol{C})$ *and* $\boldsymbol{E} \to \boldsymbol{A}^*$ *as* $\gamma \to 0$.

3.2 Perturbed-DTW Computation

Analogously, perturbed-DTW faces the computational challenge, as evaluating (8) still requires enumerating over the exponentially large space $\mathcal{A}_{m,n}$. To address this, we adapt the dynamic programming formulation of DTW by replacing the minimum operator in (3) with the perturbed minimum operator. Specifically, we define the *perturbed accumulated cost matrix* $\boldsymbol{V}$ recursively as

$$V_{i,j} = \mathbb{E}\left[\min\left\{V_{i-1,j-1} - \gamma\varepsilon_{i-1,j-1},\ V_{i-1,j} - \gamma\varepsilon_{i-1,j},\ V_{i,j-1} - \gamma\varepsilon_{i,j-1}\right\}\right] + C_{i,j}.$$

This recursive form will end at $V_{m,n}$. In this way, we just need to compute the expectation over three variables in one recursion and set $\text{perturbed-DTW}_\gamma(\boldsymbol{C}) = V_{m,n}$, which makes the computation tractable. We now examine two specific perturbation distributions: the Gumbel and the GEV.

Example: Gumbel Perturbation. The dynamic programming formula of perturbed-DTW for Gumbel noise is

$$\begin{aligned} V_{i,j} &= \mathbb{E}\left[\min\{V_{i,j-1} - \gamma\varepsilon_{i,j-1}, V_{i-1,j} - \gamma\varepsilon_{i-1,j}, V_{i-1,j-1} - \gamma\varepsilon_{i-1,j-1}\}\right] + C_{i,j} \\ &= -\gamma \log\left(\exp\left(-\tfrac{V_{i,j-1}}{\gamma}\right) + \exp\left(-\tfrac{V_{i-1,j}}{\gamma}\right) + \exp\left(-\tfrac{V_{i-1,j-1}}{\gamma}\right)\right) + C_{i,j}. \end{aligned} \tag{14}$$

which is consistent to soft-DTW. This connection casts perturbed-DTW to differentiable dynamic programming (Mensch & Blondel, 2018) and reveals that soft-DTW is a special case of Gumbel perturbations.

Proposition 4. *Define the (random) perturbed cost matrix $\widetilde{\boldsymbol{C}}_\gamma$, where $[\widetilde{\boldsymbol{C}}_\gamma]_{i,j} = C_{i,j} - \gamma\varepsilon_{i,j}$ and $\varepsilon_{i,j}$ is Gumbel$(-c, 1)$ distributed. Then*

$$\text{soft-DTW}_\gamma(\boldsymbol{C}) = \mathbb{E}\big[\,\text{DTW}(\widetilde{\boldsymbol{C}}_\gamma)\big]. \tag{15}$$

This shows that soft-DTW equals the expectation of DTW discrepancy for perturbed local cost matrix $\widetilde{\boldsymbol{C}}$ under Gumbel perturbation.

Example: Generalized Extreme Value Perturbation. Different from the linear programming formulation of perturbed-DTW in Section 3.1 , here we no longer enumerate alignments in $\mathcal{A}_{m,n}$. Instead, we just need to consider three admissible transition directions $\{\rightarrow, \downarrow, \searrow\}$ at each stage (i, j). When the perturbation vector $\boldsymbol{\varepsilon} = (\varepsilon_{i-1,j-1}, \varepsilon_{i-1,j}, \varepsilon_{i,j-1})$ follows a GEV distribution, three distinct schemes of grouping need to be considered: [2]

$$g_1 = \{\, \{\rightarrow, \downarrow\},\ \{\searrow\}\,\}, \qquad g_2 = \{\, \{\rightarrow, \searrow\},\ \{\downarrow\}\,\}, \qquad g_3 = \{\, \{\downarrow, \searrow\},\ \{\rightarrow\}\,\}.$$

To ease the illustration, we just present g_1 and a comprehensive discussion of grouping is deferred to Appendix A.4 . Formally, we divide the directions $\{\rightarrow, \downarrow, \searrow\}$ of warping paths into two groups: $J_1 = \{\downarrow, \rightarrow\}$ and $J_2 = \{\searrow\}$. The perturbation $(\varepsilon_{i-1,j-1}, \varepsilon_{i,j-1}, \varepsilon_{i-1,j})$ follows GEV distribution, then the dynamic programming formula is

$$\begin{aligned} V_{i,j} &= \mathbb{E}\left[\min\{V_{i,j-1} - \gamma\varepsilon_{i,j-1}, V_{i-1,j} - \gamma\varepsilon_{i-1,j}, V_{i-1,j-1} - \gamma\varepsilon_{i-1,j-1}\}\right] + C_{i,j} \\ &= -\gamma \log\left(\left(\exp(-\tfrac{V_{i,j-1}}{\gamma\tau}) + \exp(-\tfrac{V_{i-1,j}}{\gamma\tau})\right)^{\tau} + \exp\left(-\tfrac{V_{i-1,j-1}}{\gamma}\right)\right) + C_{i,j}. \end{aligned} \tag{16}$$

It is important to clarify that the value $V_{m,n}$ obtained via the dynamic programming recursion (16) is a tractable algorithmic realization, rather than an exact evaluation, of the theoretical ns-DTW defined in (11). This distinction can be understood from two perspectives. First, the global definition in (11) implies a single GEV perturbation of dimension $|\mathcal{A}_{m,n}|$ over the entire alignment space, whereas the DP formulation applies independent, low-dimensional GEV perturbations locally to the three transition directions at each step. Second, regarding the recursive structure: unlike the standard Log-Sum-Exp operator, which satisfies the stability property (i.e., the sum of Gumbel variables follows a Gumbel distribution), the nested application of the generalized operators in (16) does not strictly preserve the form of the global GEV distribution. Despite this theoretical distinction, we refer to the efficient DP output $V_{m,n}$ as ns-DTW throughout this work.

Effect of Grouping. The ns-DTW offers greater flexibility in modeling diverse alignment structures by allowing different groups of directions. This enables the algorithm to produce alignments that are skewed towards either the vertical ($\downarrow$) or horizontal ($\rightarrow$) directions, as illustrated in Figure 3.

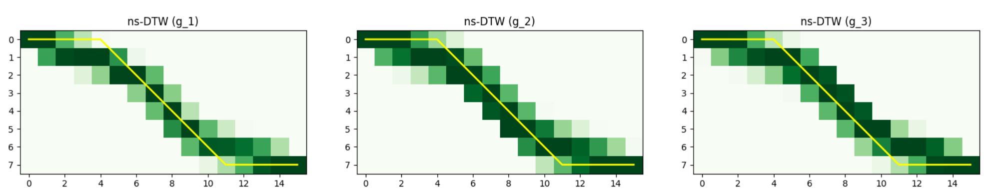

(a) ns-DTW ($g1$) (b) ns-DTW ($g2$) (c) ns-DTW ($g3$)

Figure 3: Comparison of warping paths with under different groupings of ns-DTW. The yellow path is depicted as the optimal warping path under DTW.

Effect of τ. The flexibility of ns-DTW is also governed by the parameter τ. Setting $\tau = 1$ recovers the standard soft-DTW. Conversely, as $\tau \to 0$, the model becomes increasingly selective: transitions with higher accumulated costs receive vanishing weights, while those with lower costs are emphasized. This mechanism introduces a structural skew toward the optimal path. As illustrated in Figure 4, decreasing τ progressively enlarges the expected warping path toward the direction of lower cost (e.g., the vertical direction $\downarrow$), allowing the model to adaptively prune high-cost deviations.

Proposition 3 reveals that the expected alignment pathes of perturbed-DTW, which is exactly the expected alignment matrix $\boldsymbol{E}$ under the distribution $P(\boldsymbol{A}; \boldsymbol{C})$. However, this general alignment matrix distribution is hard to compute for general perturbation $\boldsymbol{\varepsilon}$. Specifically, let transition probability tensor $\mathbf{G} \in (0, 1]^{m\times n\times 3}$. For any given (i, j), $\mathbf{G}_{i,j,:} \in \mathbb{R}^3$ specifies a stochastic alignment policy over feasible actions $\{\rightarrow, \downarrow, \searrow\}$, so that $P(A_{i,j-1} = 1) = \mathbf{G}_{i,j,1}$, $P(A_{i-1,j} = 1) = \mathbf{G}_{i,j,2}$, and $P(A_{i-1,j-1} = 1) = \mathbf{G}_{i,j,3}$. The transition probability tensor $\mathbf{G}$ can be computed as

$$\begin{aligned} \mathbf{G}_{i,j,:} &= \mathbb{E}\left[\arg\min\left\{V_{i,j-1} - \gamma\varepsilon_{i,j-1},\ V_{i-1,j} - \gamma\varepsilon_{i-1,j},\ V_{i-1,j-1} - \gamma\varepsilon_{i-1,j-1}\right\}\right] \\ &= -\gamma\nabla \log\left(\left(\exp(-\tfrac{V_{i,j-1}}{\gamma\tau}) + \exp(-\tfrac{V_{i-1,j}}{\gamma\tau})\right)^{\tau} + \exp\left(-\tfrac{V_{i-1,j-1}}{\gamma}\right)\right). \end{aligned} \tag{17}$$

[2] It can be revealed that grouping all three directions together—or placing each direction in its own group—yields the classical soft-DTW recursion.

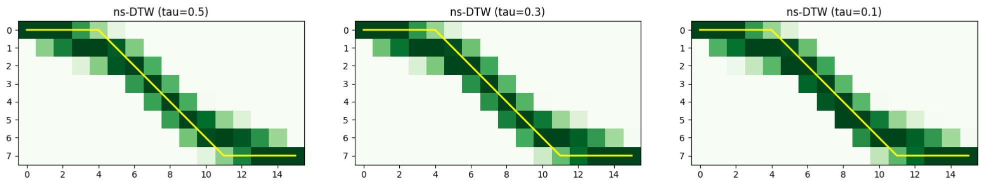

(a) ns-DTW ($\tau = 0.50$) (b) ns-DTW ($\tau = 0.3$) (c) ns-DTW ($\tau = 0.1$)

Figure 4: Comparison of warping paths with different temperature parameters τ of ns-DTW.

where the gradient is taken with respect to $\{V_{i,j-1}, V_{i-1,j}, V_{i-1,j-1}\}$. Then the expected alignment matrix is computed as

$$E_{i,j} = \mathsf{G}_{i,j+1,1} E_{i,j+1} + \mathsf{G}_{i+1,j,2} E_{i+1,j} + \mathsf{G}_{i+1,j+1,3} E_{i+1,j+1}.$$

This recursive formula can be treated as the differentiable dynamic programming with nested Shannon entropy. The ns-DTW allows the model to control the intensity (skewness) toward directions associated with lower accumulated costs, by using τ and grouping schemes to introduce skewness. By promoting a broader mixture over feasible paths, ns-DTW can approximate the true alignment cost more effectively than soft-DTW. Algorithm 1 presents the pseudocode-for computing ns-DTW and its transition probability tensor. A more detailed discussion is provided in the appendix.

Algorithm 1 ns-DTW and transition probability tensor computation

Require: Cost matrix $\boldsymbol{C} \in \mathbb{R}^{m \times n}$, $\gamma \geq 0$, $0 < \tau \leq 1$
Initialize: $V_{i,0} \leftarrow \infty$ for all i; $V_{0,j} \leftarrow \infty$ for all j; $V_{0,0} \leftarrow 0$
for $i \in [1, \ldots, m]$ and $j \in [1, \ldots, n]$ **do**
    Compute $V_{i,j}$ via (16)
    Compute $\mathsf{G}_{i,j,:}$ via (17)
end for
Return:
ns-DTW$_\gamma(\boldsymbol{C}) = V_{m,n} \in \mathbb{R}$; $\mathsf{G} \in (0, 1]^{m \times n \times 3}$

4 Applications

In this section, we conduct experiments using the UCR Time Series Classification Archive (Chen et al., 2015) . We consider a subset of the archive containing 47 datasets for average, classification[3] and clustering tasks. We report a summary of our results in the manuscript, with full details provided in the appendix.

4.1 Averaging

We investigate the problem of computing Fréchet mean of time series with respect to ns-DTW. Given a collection of time series: $\mathbf{y}_1, \ldots, \mathbf{y}_M$, our goal is to compute a barycenter $\mathbf{x}$ that minimizes the total ns-DTW discrepancy:

$$\min_{\mathbf{x} \in \mathbb{R}^{p \times m}} \sum_{i=1}^{M} \text{ns-DTW}(\boldsymbol{C}(\mathbf{x}, \mathbf{y}_i))$$

We evaluate the quality of the barycenters in terms of DTW discrepancy and compare ns-DTW with several established baselines, including subgradient method (Schultz & Jain, 2018), DBA (Petitjean et al., 2011) and soft-DTW (Cuturi & Blondel, 2017) methods.

We evaluate the methods based on three direction grouping schemes: $\{g_1, g_2, g_3\}$, parameters $\tau \in \{0.80, 0.85, 0.90, 0.95\}$ and $\gamma \in \{0.1, 0.01, 0.001, 0.0001\}$. Table 1 summarizes the barycenter

[3]As some datasets contain only one class, we use 43 datasets for the classification task.

averaging results across varying γ. By selecting the optimal grouping scheme g_i and parameter τ, ns-DTW demonstrates robust performance improvements. Specifically, it achieves a lower objective value than the Subgradient method on **100%** of datasets and DBA on **97.87%**. Furthermore, when compared against the strongest baseline, soft-DTW (both methods tuned for optimal γ), ns-DTW yields superior results on **74.47%** of the datasets. Qualitative results on the *Beef* dataset are visualized in Figure 5. Comprehensive dataset-wise results are provided in Appendix B.1.

Table 1: Percentage of the datasets on which the proposed ns-DTW barycenter is achieving lower DTW loss than competing methods.

	subgradient	DBA	soft-DTW
$\gamma = 0.1$	68.09%	46.81%	36.17%
$\gamma = 0.01$	80.85%	72.34%	59.57%
$\gamma = 0.001$	95.74%	87.23%	80.85%
$\gamma = 0.0001$	100.00%	91.49%	91.49%

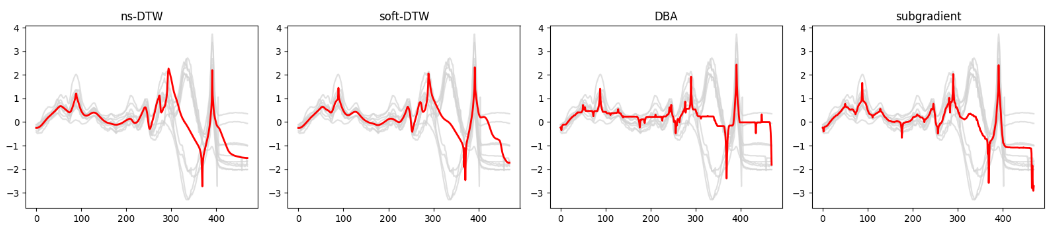

Figure 5: Comparison of barycenters obtained by ns-DTW, soft-DTW and DBA methods on the UCR time series *Beef* dataset, using Euclidean averaging for initialization.

4.2 Classification

Nearest Centroid Classifier. We evaluated time series classification performance using the *Nearest Centroid Classifier* (NCC), where class centroids were computed as barycenters using the respective averaging algorithms. We employed a 50%/25%/25% train-validation-test split, with the smoothing parameter $\gamma \in \{0.1, 0.01, 0.001, 0.0001\}$ selected via cross-validation.

Overall, ns-DTW demonstrated superior performance, achieving equal or higher accuracy compared to Subgradient methods on **93.02%** of datasets, DBA on **88.37%**, and soft-DTW on **86.05%**. Figure 6 presents the pairwise performance comparison between ns-DTW and baselines for NCC classification.

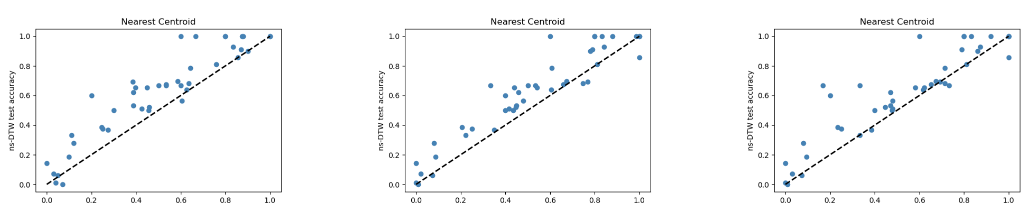

(a) Subgradient v.s. ns-DTW (b) DBA v.s. ns-DTW (c) soft-DTW v.s. ns-DTW

Figure 6: Points above the diagonal indicate datasets where the ns-DTW outperforms (a) subgradient; (b)DBA; (c) soft-DTW in nearest centroid classifier.

1NN Classifier. We also evaluated the *1-Nearest Neighbor (1NN)* classifier, where test samples are assigned to the class of the nearest training example based on the minimized DTW discrepancy. The data splits and cross-validation for γ remained consistent with the NCC experiments.

Overall, ns-DTW achieved equal or higher accuracy compared to DBA on **88.37%** of datasets and soft-DTW on **86.05%**.

4.3 CLUSTERING

We study the k-means clustering task: the distances between each time series are ns-DTW discrepancy and the centroids of each class are their barycenters. Formally, the objective is to find clusters $C_1, \ldots, C_K$ that minimize total within-cluster ns-DTW discrepancy:

$$\min_{C_1,\ldots,C_K} \sum_{k=1}^{K} \sum_{i,j \in C_k} \text{ns-DTW}(\boldsymbol{C}(\mathbf{y}_i, \mathbf{y}_j)).$$

Overall, ns-DTW achieved equal or higher accuracy compared to DBA on **88.37%** of datasets and soft-DTW on **86.05%**. Our ns-DTW outperforms DBA on **100.00%** and soft-DTW on **76.60%**. Figure 7 presents the clustering results on the *CBF* dataset and the complete results are shown in Appendix B.4.

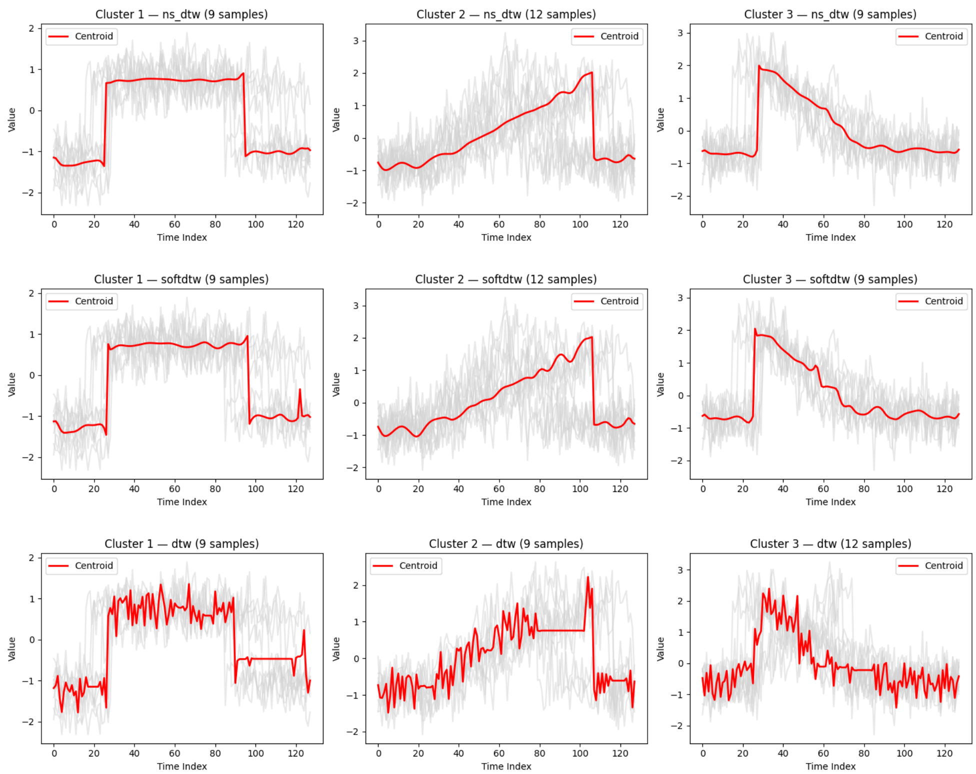

Figure 7: Comparison of clustering results obtained by ns-DTW (first row), soft-DTW (second row) and DBA (third row) methods on the UCR time series *CBF* dataset, initialized using Euclidean averaging.

5 CONCLUSION

We introduced *perturbed-DTW*, a probabilistic framework that makes DTW differentiable by adding random perturbations to the warping costs. This perspective recovers soft-DTW under Gumbel perturbation, providing a natural probabilistic interpretation. Extending to the generalized extreme value family leads to *nested soft-DTW*, which enables tunable skewness in alignments and greater modeling flexibility.

Experiments on barycenter computation and clustering demonstrate competitive performance over existing methods. Looking forward, extending perturbed-DTW to divergence-based formulations and to broader classes of perturbed dynamic programming operators offers promising directions for future work.

ACKNOWLEDGMENTS

Xiangqian Sun was supported by grant from XJTLU Research Development Fund [RDF-23-02-052]. Chaoqun Wang was supported by grant from XJTLU Research Development Fund [RDF-24-02-033]. Wei Zhang was partly supported by grants from the National Natural Science Foundation of China [Grants 72401257, 72431010 , 71821002];

ETHICS STATEMENT

This research does not raise any potential violations of the ICLR Code of Ethics. In particular, it does not involve human subjects, dataset release practices, or potentially harmful insights, methodologies, or applications. It also raises no concerns regarding conflicts of interest or sponsorship, discrimination, bias, or fairness, nor does it present issues related to privacy, security, legal compliance, or research integrity (e.g., IRB approval, documentation, or research ethics).

REPRODUCIBILITY STATEMENT

The datasets used in this research are publicly available at `https://www.cs.ucr.edu/~eamonn/time_series_data/`, and the code for reproducing our results is provided in the supplementary material.

REFERENCES

Richard Bellman. On the theory of dynamic programming. *Proceedings of the national Academy of Sciences*, 38(8):716–719, 1952.

Serge Belongie, Jitendra Malik, and Jan Puzicha. Shape matching and object recognition using shape contexts. *IEEE transactions on pattern analysis and machine intelligence*, 24(4):509–522, 2002.

Donald J Berndt and James Clifford. Using dynamic time warping to find patterns in time series. In *Proceedings of the 3rd international conference on knowledge discovery and data mining*, pp. 359–370, 1994.

Quentin Berthet, Mathieu Blondel, Olivier Teboul, Marco Cuturi, Jean-Philippe Vert, and Francis Bach. Learning with differentiable pertubed optimizers. *Advances in Neural Information Processing Systems*, 33:9508–9519, 2020.

Mathieu Blondel, André FT Martins, and Vlad Niculae. Learning with fenchel-young losses. *Journal of Machine Learning Research*, 21(35):1–69, 2020.

Mathieu Blondel, Arthur Mensch, and Jean-Philippe Vert. Differentiable divergences between time series. In *International Conference on Artificial Intelligence and Statistics*, pp. 3853–3861. PMLR, 2021.

Milutin Brankovic, Kevin Buchin, Koen Klaren, André Nusser, Aleksandr Popov, and Sampson Wong. (k, l)-medians clustering of trajectories using continuous dynamic time warping. In *Proceedings of the 28th International Conference on Advances in Geographic Information Systems*, pp. 99–110, 2020.

Chien-Yi Chang, De-An Huang, Yanan Sui, Li Fei-Fei, and Juan Carlos Niebles. D3tw: Discriminative differentiable dynamic time warping for weakly supervised action alignment and segmentation. In *Proceedings of the IEEE/CVF Conference on Computer Vision and Pattern Recognition*, pp. 3546–3555, 2019.

Yanping Chen, Eamonn Keogh, Bing Hu, Nurjahan Begum, Anthony Bagnall, Abdullah Mueen, and Gustavo Batista. The ucr time series classification archive, July 2015. `www.cs.ucr.edu/~eamonn/time_series_data/`.

Marco Cuturi and Mathieu Blondel. Soft-dtw: a differentiable loss function for time-series. In *International conference on machine learning*, pp. 894–903. PMLR, 2017.

Marco Cuturi, Jean-Philippe Vert, Oystein Birkenes, and Tomoko Matsui. A kernel for time series based on global alignments. In *2007 IEEE International Conference on Acoustics, Speech and Signal Processing-ICASSP'07*, volume 2, pp. II–413. IEEE, 2007.

Mogens Fosgerau, Emerson Melo, Andre De Palma, and Matthew Shum. Discrete choice and rational inattention: A general equivalence result. *International economic review*, 61(4):1569–1589, 2020.

Fumitada Itakura. Minimum prediction residual principle applied to speech recognition. *IEEE Transactions on acoustics, speech, and signal processing*, 23(1):67–72, 2003.

Vincent Le Guen and Nicolas Thome. Shape and time distortion loss for training deep time series forecasting models. *Advances in neural information processing systems*, 32, 2019.

Daniel McFadden. Econometric models of probabilistic choice. *Structural analysis of discrete data with econometric applications*, 198272, 1981.

Arthur Mensch and Mathieu Blondel. Differentiable dynamic programming for structured prediction and attention. In *International Conference on Machine Learning*, pp. 3462–3471. PMLR, 2018.

François Petitjean, Alain Ketterlin, and Pierre Gançarski. A global averaging method for dynamic time warping, with applications to clustering. *Pattern recognition*, 44(3):678–693, 2011.

Chotirat Ann Ratanamahatana and Eamonn Keogh. Making time-series classification more accurate using learned constraints. In *Proceedings of the 2004 SIAM international conference on data mining*, pp. 11–22. SIAM, 2004.

Hiroto Saigo, Jean-Philippe Vert, and Tatsuya Akutsu. Optimizing amino acid substitution matrices with a local alignment kernel. *BMC bioinformatics*, 7(1):246, 2006.

Hiroaki Sakoe and Seibi Chiba. Dynamic programming algorithm optimization for spoken word recognition. *IEEE transactions on acoustics, speech, and signal processing*, 26(1):43–49, 2003.

David Schultz and Brijnesh Jain. Nonsmooth analysis and subgradient methods for averaging in dynamic time warping spaces. *Pattern recognition*, 74:340–358, 2018.

Xiangqian Sun, Cheuk Hang Leung, Yijun Li, and Qi Wu. A unified perspective on regularization and perturbation in differentiable subset selection. In *International Conference on Artificial Intelligence and Statistics*, pp. 4629–4642. PMLR, 2023.

Kenneth E Train. *Discrete choice methods with simulation*. Cambridge university press, 2009.

Jiawen Zhang, Shun Zheng, Wei Cao, Jiang Bian, and Jia Li. Warpformer: A multi-scale modeling approach for irregular clinical time series. In *Proceedings of the 29th ACM SIGKDD Conference on Knowledge Discovery and Data Mining*, pp. 3273–3285, 2023.

Zheng Zhang, Romain Tavenard, Adeline Bailly, Xiaotong Tang, Ping Tang, and Thomas Corpetti. Dynamic time warping under limited warping path length. *Information Sciences*, 393:91–107, 2017.

A Proofs and Computations

A.1 Proof of Theorem 1

We first show the following result.

Lemma 2. *Let*

$$M \ := \max_{j\in[J],\, k\in[K_j]} \{\mu_{jk} + \varepsilon_{jk}\},$$

with ε following the GEV joint distribution

$$F(\varepsilon_{11}, \ldots, \varepsilon_{JK_J}) = \exp\left(-\sum_{j=1}^{J} \Big[\sum_{k=1}^{K_j} \exp\Big(-\frac{\varepsilon_{jk}}{\tau_j} \Big) \Big]^{\tau_j} \right).$$

Then

$$\mathbb{E}[M] \ = \left(\sum_{j=1}^{J} \left(\sum_{k=1}^{K_j} \exp\left(\frac{\mu_{jk}}{\tau_j} \right) \right)^{\tau_j} \right).$$

Proof. For any $t \in \mathbb{R}$,

$$\begin{aligned}
\Pr(M \le t) &= \Pr(\varepsilon_{jk} \le t - \mu_{jk} \ \forall j, k) \\
&= F(t - \mu_{11}, \ldots, t - \mu_{JK_J}) \\
&= \exp\left(-\sum_{j=1}^{J} \Big[\sum_{k=1}^{K_j} \exp\Big(-\frac{t - \mu_{jk}}{\tau_j} \Big) \Big]^{\tau_j} \right) \\
&= \exp\left(-\sum_{j=1}^{J} \Big[e^{-t/\tau_j} \sum_{k=1}^{K_j} e^{\mu_{jk}/\tau_j} \Big]^{\tau_j} \right) \\
&= \exp\left(-e^{-t} \sum_{j=1}^{J} \Big(\sum_{k=1}^{K_j} e^{\mu_{jk}/\tau_j} \Big)^{\tau_j} \right).
\end{aligned}$$

Define

$$\Omega(\mu) = \log \left(\sum_{j=1}^{J} \Big(\sum_{k=1}^{K_j} e^{\mu_{jk}/\tau_j} \Big)^{\tau_j} \right).$$

Then

$$\Pr(M \le t) = \exp\big(-\exp\big(-(t - \Omega(\mu)) \big) \big),$$

so M is Gumbel distributed with location $\Omega(\mu)$ and scale 1. By property of Gumbel distribution, we know that

$$\mathbb{E}[M] = \Omega(\mu) + c,$$

where $c \approx 0.5772$ is the Euler-Mascheroni constant. If the GEV errors are centered to have mean zero (i.e. $\tilde{\varepsilon}_{jk} = \varepsilon_{jk} - c$), then

$$\mathbb{E}\Big[\max_{j,k} \{\mu_{jk} + \tilde{\varepsilon}_{jk}\} \Big] = \Omega(\mu).$$

□

Next, we give the proof of Theorem 1.

Proof. If the GEV errors are centered to have mean zero (i.e. $\tilde{\varepsilon}_{jk} = \varepsilon_{jk} - c$),

$$\begin{aligned}
\text{perturbed-DTW}_\gamma(C) &\coloneqq \mathbb{E}\left[\min_{A\in\mathcal{A}_{m,n}} \left\{\langle A, C\rangle - \gamma\tilde{\boldsymbol{\varepsilon}}\right\}\right] \\
&= -\gamma\mathbb{E}\left[\max_{A\in\mathcal{A}_{m,n}} \left\{-\frac{\langle A, C\rangle}{\gamma} + \tilde{\boldsymbol{\varepsilon}}\right\}\right] \\
&= -\gamma\log\left(\sum_{\ell=1}^{J}\left(\sum_{A\in J}\exp\left(-\frac{\langle A, C\rangle}{\gamma\tau_\ell}\right)\right)^{\tau_\ell}\right),
\end{aligned}$$

where the last equality comes from Lemma 2. Denote $s_{jk} = \langle A, C\rangle$ if A is the kth one in group j. The probability distritution of alignment matrix is

$$\begin{aligned}
P_{jk} &= \frac{\partial}{\partial s_{jk}}\left[-\gamma\log\left(\sum_{\ell=1}^{J}\left(\sum_{A\in J}\exp\left(-\frac{s_{jk}}{\gamma\tau_\ell}\right)\right)^{\tau_\ell}\right)\right] \\
&= \frac{\left(\sum_{m=1}^{K_j}\exp\left(\frac{s_{jm}}{\gamma\tau_j}\right)\right)^{\tau_j-1}}{\sum_{\ell=1}^{J}\left(\sum_{m=1}^{K_\ell}\exp\left(\frac{s_{\ell m}}{\gamma\tau_\ell}\right)\right)^{\tau_\ell}}\exp\left(\frac{s_{jk}}{\gamma\tau_j}\right),
\end{aligned}$$

as desired. □

A.2 Proof of Proposition 2

Proof. For simplicity, we just show the case $\gamma = 1$. The Lagrangian function is defined as

$$L(\boldsymbol{p}, \lambda) = \langle \boldsymbol{p}, \boldsymbol{s}(C)\rangle + H(\boldsymbol{p}) + \lambda(\sum_\ell\sum_m p_{\ell m} - 1). \tag{18}$$

The optimality condition gives

$$\begin{cases} s_{\ell m} + \tau_\ell(1 + \log p_{\ell m}) - (\tau_\ell - 1)(1 + \sum_m p_{\ell m}) + \lambda = 0, \quad \forall \ell, m \\ \sum_\ell\sum_m p_{\ell m} = 1. \end{cases} \tag{19}$$

Equation 19 implies

$$p_{\ell m} = \exp\left(\frac{-s_{\ell m} - 1 - \lambda}{\tau_\ell} + \frac{\tau_\ell - 1}{\tau_\ell}\log\sum_m p_{\ell m}\right). \tag{20}$$

With a little abuse of notations, we denote $p_\ell = \sum_m p_{\ell m}$. Then

$$p_\ell = \sum_m p_{\ell m} = \sum_m \exp\left(\frac{-s_{\ell m} - 1 - \lambda}{\tau_\ell} + \frac{\tau_\ell - 1}{\tau_\ell}\log\sum_m p_{\ell m}\right) \tag{21}$$

$$= \sum_m \exp\left(\frac{-s_{\ell m} - 1 - \lambda}{\tau_\ell} + \frac{\tau_\ell - 1}{\tau_\ell}\log p_\ell\right) \tag{22}$$

$$\Longrightarrow \frac{1}{\tau_\ell}\log p_\ell = \log\sum_m \exp(\frac{-s_{\ell m} - 1 - \lambda}{\tau_\ell}). \tag{23}$$

By leveraging the equality condition, we have

$$1 = \sum_\ell p_\ell = \sum_\ell\left(\sum_m \exp(\frac{-s_{\ell m} - 1 - \lambda}{\tau_\ell})\right)^{\tau_\ell} = \sum_\ell\left(\sum_m \exp(\frac{-s_{\ell m}}{\tau_\ell})\right)^{\tau_\ell} / \exp(1 + \lambda) \tag{24}$$

$$\Longrightarrow \lambda = \log\left(\sum_\ell\left(\sum_m \exp(\frac{-s_{\ell m}}{\tau_\ell})\right)^{\tau_\ell}\right) - 1. \tag{25}$$

By substituting (23) and (25) into (20), we have

$$\begin{aligned} p_{\ell m} &= \exp\left(\frac{-s_{\ell m}}{\tau_\ell} - \frac{1}{\tau_\ell} - \frac{\lambda}{\tau_\ell} + (\tau_\ell - 1)\log\sum_m \exp\left(\frac{-s_{\ell m}}{\tau_\ell}\right) - 1 + \frac{1}{\tau_\ell} - \lambda + \frac{\lambda}{\tau_\ell}\right) \\ &= \exp\left(\frac{-s_{\ell m}}{\tau_\ell} + (\tau_\ell - 1)\log\sum_m \exp\left(\frac{-s_{\ell m}}{\tau_\ell}\right) - \log\left(\sum_\ell\left(\sum_m \exp(\frac{-s_{\ell m}}{\tau_\ell})\right)^{\tau_\ell}\right)\right). \end{aligned} \tag{26}$$

The proof completes by plugging (26) into (6). □

A.3 Proof of Proposition 3

The fourth property is straightforward; here, we present only the first three.

Proof. 1. By definition of perturbed-DTW, we have

$$\begin{aligned} \text{perturbed-DTW}_\gamma(\boldsymbol{C}) &= \mathbb{E}_{\boldsymbol{\varepsilon}\sim\mathbb{P}}\left[\min\left\{\langle \mathbf{A}, \mathbf{C}\rangle - \gamma\boldsymbol{\varepsilon}\right\}\right] \\ &= \gamma\mathbb{E}_{\boldsymbol{\varepsilon}\sim\mathbb{P}}\left[\min\left\{\frac{1}{\gamma}\langle \mathbf{A}, \mathbf{C}\rangle - \boldsymbol{\varepsilon}\right\}\right] \\ &= \gamma\,\text{perturbed-DTW}_1(\boldsymbol{C}/\gamma). \end{aligned}$$

2. The optimal alignment matrix $\boldsymbol{A}$ follows

$$\begin{aligned} P(\boldsymbol{A};\boldsymbol{C}) &= P\Big(\langle \boldsymbol{A}, \boldsymbol{C}\rangle - \gamma\varepsilon \le \langle \boldsymbol{A}', \boldsymbol{C}\rangle - \gamma\varepsilon', \forall \boldsymbol{A}', \varepsilon'\Big) \\ &= \mathbb{E}\left[\arg\min_{\boldsymbol{A}}\left\{(\langle \mathbf{A}, \mathbf{C}\rangle) - \gamma\boldsymbol{\varepsilon}\right\}\right]. \end{aligned}$$

3. By the Williams–Daly–Zachary theorem (McFadden, 1981),

$$\begin{aligned} \nabla_{\boldsymbol{C}}\,\text{perturbed-DTW}_\gamma(\boldsymbol{C}) &= \Big\langle\ \mathbb{E}\left[\arg\min_{\langle \boldsymbol{A}, \boldsymbol{C}\rangle}\left\{\langle \mathbf{A}, \mathbf{C}\rangle - \gamma\boldsymbol{\varepsilon}\right\}\right], \nabla_{\boldsymbol{C}}\langle \boldsymbol{A}, \boldsymbol{C}\rangle\ \Big\rangle \\ &= \sum_{\boldsymbol{A}\in\mathcal{A}_{m,n}} \mathbb{E}\left[\arg\min_{\boldsymbol{A}\in\mathcal{A}_{m,n}}\left\{\langle \mathbf{A}, \mathbf{C}\rangle - \gamma\boldsymbol{\varepsilon}\right\}\right]\cdot \boldsymbol{A} \\ &= \sum_{\boldsymbol{A}\in\mathcal{A}_{m,n}} P(\boldsymbol{A};\boldsymbol{C})\cdot\boldsymbol{A} = \boldsymbol{E}. \end{aligned}$$

□

A.4 General Formulation of ns-DTW

As discussed earlier, ns-DTW can be viewed as a generalized perturbed variant of soft-DTW obtained by replacing the Gumbel perturbation with a GEV perturbation. Note that the GEV distribution can be regarded as multivariate generalization of the Gumbel distribution with groupwise correlation. This substitution introduces not only a hyper-parameter τ but also multiple schemes of direction groupings. The dynamic programming formula for general perturbed-DTW is

$$V_{i,j} = \mathbb{E}\Big[\min\Big\{V_{i-1,j-1} - \gamma\varepsilon_{i-1,j-1},\ V_{i-1,j} - \gamma\varepsilon_{i-1,j},\ V_{i,j-1} - \gamma\varepsilon_{i,j-1}\Big\}\Big] + C_{i,j}.$$

When the perturbation vector $\boldsymbol{\varepsilon} = (\varepsilon_{i-1,j-1},\ \varepsilon_{i-1,j},\ \varepsilon_{i,j-1})$ follows a GEV distribution, three distinct grouping schemes need to be considered: [4]

$$g_1 = \big\{\,\{\rightarrow,\downarrow\},\ \{\searrow\}\,\big\}, \qquad g_2 = \big\{\,\{\rightarrow,\searrow\},\ \{\downarrow\}\,\big\}, \qquad g_3 = \big\{\,\{\downarrow,\searrow\},\ \{\rightarrow\}\,\big\}.$$

[4]It can be revealed that grouping all three directions together—or placing each direction in its own group—yields the classical soft-DTW recursion.

Therefore, the general formulas for dynamic-programming recursions for different grouping schemes are

$$g_1: \quad V_{i,j} = -\gamma \log\Big[\Big(e^{-V_{i,j-1}/(\gamma\tau)} + e^{-V_{i-1,j}/(\gamma\tau)}\Big)^{\tau} + e^{-V_{i-1,j-1}/\gamma}\Big] + C_{i,j}, \tag{27}$$

$$g_2: \quad V_{i,j} = -\gamma \log\Big[\Big(e^{-V_{i,j-1}/(\gamma\tau)} + e^{-V_{i-1,j-1}/(\gamma\tau)}\Big)^{\tau} + e^{-V_{i-1,j}/\gamma}\Big] + C_{i,j}, \tag{28}$$

$$g_3: \quad V_{i,j} = -\gamma \log\Big[\Big(e^{-V_{i-1,j}/(\gamma\tau)} + e^{-V_{i-1,j-1}/(\gamma\tau)}\Big)^{\tau} + e^{-V_{i,j-1}/\gamma}\Big] + C_{i,j}. \tag{29}$$

A.5 NS-DTW COMPUTATION

To streamline the presentation, we focus on the ns-DTW computation under the first scheme of grouping g_1. The transition probabilities and gradients for the remaining groupings can be derived analogously. The dynamic programming formula of perturbed-DTW under GEV perturbation in g_1 is

$$\begin{aligned} V_{i,j} &= \mathbb{E}\left[\min\{V_{i,j-1} + C_{i,j} - \gamma\varepsilon_{i,j-1}, V_{i-1,j} + C_{i,j} - \gamma\varepsilon_{i-1,j}, V_{i-1,j-1} + C_{i,j} - \gamma\varepsilon_{i-1,j-1}\}\right] \\ &= -\gamma \log\left(\left(\exp(-\tfrac{V_{i,j-1}}{\gamma\tau}) + \exp(-\tfrac{V_{i-1,j}}{\gamma\tau})\right)^{\tau} + \exp\left(-\tfrac{V_{i-1,j-1}}{\gamma}\right)\right) + C_{i,j}. \end{aligned} \tag{30}$$

Therefore, the transition probability is

$$P(A_{i,j-1}=1) = \boldsymbol{G}_{i,j,1} = \frac{\left(\exp(-\frac{V_{i,j-1}}{\gamma\tau}) + \exp(-\frac{V_{i-1,j}}{\gamma\tau})\right)^{\tau-1}}{\left(\exp(-\frac{V_{i,j-1}}{\gamma\tau}) + \exp(-\frac{V_{i-1,j}}{\gamma\tau})\right)^{\tau} + \exp\left(-\frac{V_{i-1,j-1}}{\gamma}\right)} \cdot \exp\left(-\frac{V_{i,j-1}}{\gamma\tau}\right),$$

$$P(A_{i-1,j}=1) = \boldsymbol{G}_{i,j,2} = \frac{\left(\exp(-\frac{V_{i,j-1}}{\gamma\tau}) + \exp(-\frac{V_{i-1,j}}{\gamma\tau})\right)^{\tau-1}}{\left(\exp(-\frac{V_{i,j-1}}{\gamma\tau}) + \exp(-\frac{V_{i-1,j}}{\gamma\tau})\right)^{\tau} + \exp\left(-\frac{V_{i-1,j-1}}{\gamma}\right)} \cdot \exp\left(-\frac{V_{i-1,j}}{\gamma\tau}\right),$$

$$P(A_{i-1,j-1}=1) = \boldsymbol{G}_{i,j,3} = \frac{\exp\left(-\frac{V_{i-1,j-1}}{\gamma}\right)}{\left(\exp(-\frac{V_{i,j-1}}{\gamma\tau}) + \exp(-\frac{V_{i-1,j}}{\gamma\tau})\right)^{\tau} + \exp\left(-\frac{V_{i-1,j-1}}{\gamma}\right)}.$$

Then the expected alignment matrix is computed by

$$E_{i,j} = \boldsymbol{G}_{i,j+1,1}E_{i,j+1} + \boldsymbol{G}_{i+1,j,2}E_{i+1,j} + \boldsymbol{G}_{i+1,j+1,3}E_{i+1,j+1}.$$

Algorithm 2 presents the pseudocode for computing gradient of ns-DTW.

Algorithm 2 ns-DTW gradient computation

Require: $\mathbf{G} \in (0,1]^{m\times n\times 3}$ (Algorithm 1)
1: Initialize: $E_{m+1,:} \leftarrow 0$, $E_{:,n+1} \leftarrow 0$, $E_{m+1,n+1} \leftarrow 1$
2: Initialize: $\boldsymbol{G}_{m+1,:,:} \leftarrow (0,0,0)$, $\boldsymbol{G}_{:,n+1,:} \leftarrow (0,0,0)$, $\boldsymbol{G}_{m+1,n+1,:} \leftarrow (0,1,0)$
3: **for** $i \in [m,\dots,1], j \in [n,\dots,1]$, **do**
4: $\quad E_{i,j} \leftarrow \boldsymbol{G}_{i,j+1,1} \cdot E_{i,j+1} + \boldsymbol{G}_{i+1,j+1,2} \cdot E_{i+1,j+1} + \boldsymbol{G}_{i+1,j,3} \cdot E_{i+1,j}$
5: **end for**
6: **Return:** $\nabla_C \text{ns-DTW}_\gamma(C) = \boldsymbol{E} \in (0,1]^{m\times n}$

Consider the warping cost $\boldsymbol{C} \in \mathbb{R}^{m\times n}$, to compute the value of ns-DTW, Algorithm 1 requires $O(mn)$ operations and $O(mn)$ storage cost as well. This is as same as the soft-DTW. However, if we consider different groupings, in other words, dividing directions into two groups , the computational cost would be three times as soft-DTW. (since soft-DTW can be treated as one special grouping of ns-DTW).

A.6 Implementation Details and Experimental Setup

Software Environment. All experiments were implemented in **Python 3.9**. The core logic relies on `tslearn` (v0.6.4) for time series operations, `numpy` (v2.0.2) and `pandas` (v2.3.3) for data manipulation, and `scikit-learn` (v1.6.1) for evaluation metrics.

Hyperparameter Configuration. To ensure reproducibility and fair comparison, we standardized the search space and initialization protocols across all datasets. We utilized Euclidean averaging for initialization and set a maximum budget of 30 iterations for the barycenter computation, observing convergence in most cases within this limit. The specific hyperparameter ranges and grouping schemes for ns-DTW are detailed in Table 2.

Table 2: Summary of experimental settings and hyperparameter search spaces.

Parameter	Value / Definition
Software	Python 3.9, tslearn 0.6.4, numpy 2.0.2, sklearn 1.6.1
Parameter (τ)	$\{0.80,\ 0.85,\ 0.90,\ 0.95\}$
Smoothing (γ)	$\{0.1, 0.01, 0.001, 0.0001\}$
Grouping Schemes	$g_1 = \{\{\rightarrow, \downarrow\}, \{\searrow\}\}$ $g_2 = \{\{\rightarrow, \searrow\}, \{\downarrow\}\}$ $g_3 = \{\{\downarrow, \searrow\}, \{\rightarrow\}\}$
Initialization	Euclidean Averaging
Max Iterations	30

We clarify the hyperparameter selection procedure for two types of tasks: averaging and clustering(unsupervised), and classification (supervisd). Detailed results are presented in Appendix B.

Averaging and Clustering Tasks: For these tasks, we use a grid search to evaluate combinations of grouping schemes ($g_i \in \{g_1, g_2, g_3\}$), parameter $\tau \in \{0.80, 0.85, 0.90, 0.95\}$ and the parameter $\gamma \in \{0.1, 0.01, 0.001, 0.0001\}$. In other words, we evaluate all datasets for every possible combination of (g_i, τ, γ).
To examine the **effect of** g_i, we fixed each grouping scheme and then found the best τ and γ combination within the grid search that yielded the lowest DTW losses. These results are presented in the last three columns of Tables 3 and 6.
To examine the **effect of** τ, we collected results for fixed τ and g_i, then selected the γ that achieved the lowest DTW losses. The detailed results for averaging are in Appendix C (Table 7 for g_1, Table 8 for g_2, and Table 9 for g_3). For clustering, results are in Appendix E (Table 13 for g_1, Table 14 for g_2, and Table 15 for g_3).

Classification Task: For classification, we still perform a grid search over $g_i \in \{g_1, g_2, g_3\}$ and $\tau \in \{0.80, 0.85, 0.90, 0.95\}$. However, for each $\{g_i, \tau\}$ pair, γ is selected via cross-validation on the training set. This approach allows us to specifically evaluate the effects of different grouping schemes and τ while ensuring γ is optimally tuned for each combination.
To examine the **effect of** g_i, we fixed each grouping scheme and then found the best τ (with γ determined by cross-validation) within the grid search that yielded the highest classification accuracy. The results of g_i on classification performance are presented in the last three columns of Table 4.
To examine the **effect of** τ, we collected results for fixed τ and g_i, then selected the γ that achieved the highest classification accuracy. Further results showing the effects of different groupings and τ with cross-validated γ are provided in Appendix D (Table 10 for g_1, Table 11 for g_2, and Table 12 for g_3) .

B RESULTS

B.1 AVERAGING

Table 3: UCR Barycenter DTW Losses

Dataset	subgradient	DBA	soft-DTW	ns-DTW (g_1)	ns-DTW (g_2)	ns-DTW (g_3)
Adiac	0.2594	0.2576	0.2552	**0.2551**	0.2553	0.2552
ArrowHead	1.2413	1.1893	**1.1440**	1.1646	1.1640	1.1545
Beef	8.4287	4.1666	**4.0666**	4.1005	4.1025	4.1015
BeetleFly	4.9672	4.5245	4.2886	4.1907	4.1909	**4.1905**
BirdChicken	4.9910	2.4679	**2.3858**	2.3930	2.3921	2.3938
CBF	4.3019	3.8861	**3.4473**	3.7857	3.8222	3.7833
Car	0.6908	0.6703	**0.5948**	0.5954	0.5964	0.5963
ChlorineConcentration	3.6285	3.4941	3.4297	**3.4047**	3.4061	3.4091
CinCECGTorso	17.9134	8.8686	**8.3582**	8.3653	8.3597	8.3599
Coffee	0.6249	0.5950	**0.5872**	0.5890	0.5892	0.5893
Computers	17.2013	14.8046	**14.6065**	14.6314	14.6228	14.6203
CricketX	7.9406	5.9852	5.7930	5.6919	5.7399	**5.6772**
CricketY	6.3425	5.7147	**5.5186**	5.5646	5.5598	5.5645
CricketZ	6.2965	5.4289	5.3826	5.3563	5.3752	**5.3454**
DiatomSizeReduction	0.2529	0.2357	0.2282	**0.2278**	0.2278	0.2278
DistalPhalanxOutlineAgeGroup	0.7220	0.7073	0.7043	**0.7036**	0.7038	0.7038
DistalPhalanxOutlineCorrect	0.6972	0.6670	**0.6658**	0.6662	0.6662	0.6662
DistalPhalanxTW	0.3622	0.3478	**0.3448**	0.3458	0.3458	0.3458
ECG200	2.7862	2.7185	2.6750	**2.6470**	2.6537	2.6704
ECG5000	2.2571	2.2061	2.2012	**2.1968**	2.2024	2.2023
ECGFiveDays	2.7898	2.5564	2.5618	2.5275	**2.4869**	2.5243
Earthquakes	12.2798	10.7766	**10.6706**	10.7192	10.7052	10.7222
FaceAll	3.2504	2.9970	**2.8392**	2.8917	2.9055	2.8971
FaceFour	5.6599	5.3963	**5.2482**	5.3374	5.3145	5.3444
GunPoint	2.2964	**1.6673**	1.7319	1.6998	1.7036	1.7078
Ham	4.4250	4.1339	**4.0861**	4.0997	4.0929	4.0984
MedicalImages	2.7714	**2.6551**	2.6738	2.6693	2.6675	2.6693
MiddlePhalanxOutlineAgeGroup	0.5451	0.5206	0.5138	0.5120	**0.5120**	0.5143
MiddlePhalanxOutlineCorrect	0.6671	0.6423	0.6343	0.6341	0.6341	**0.6334**
MiddlePhalanxTW	0.3322	0.3284	0.3190	0.3188	0.3189	**0.3187**
MoteStrain	4.3593	4.2874	4.2537	**4.2381**	4.2390	4.2453
ProximalPhalanxTW	0.3773	0.3402	**0.3365**	0.3383	0.3378	0.3382
RefrigerationDevices	11.5572	8.5680	**7.4193**	7.9655	7.9086	7.8243
ScreenType	13.8207	12.2042	12.1071	**12.0787**	12.0857	12.0816
ShapeletSim	12.2430	11.3275	11.0399	11.0316	**11.0313**	11.0834
ShapesAll	1.2198	1.0711	1.0687	**1.0652**	1.0653	1.0690
SmallKitchenAppliances	13.0036	10.3012	**9.2726**	9.3408	9.3408	9.3398
SonyAIBORobotSurface1	1.7197	1.6757	1.6536	**1.6075**	1.6088	1.6397
SonyAIBORobotSurface2	2.7282	2.6203	2.5849	**2.5633**	2.5633	2.5633
SyntheticControl	4.5651	4.1545	4.1459	4.1092	4.0827	**4.0813**
Trace	1.8690	0.9323	0.8951	0.8954	**0.8499**	0.8699
TwoLeadECG	0.9302	0.8615	0.8463	0.8444	**0.8442**	0.8473
Wine	0.3271	**0.3239**	0.3257	0.3245	0.3251	0.3240
Worms	14.1987	10.5608	10.0867	9.9822	9.9110	**9.9007**
WormsTwoClass	9.8468	8.7107	**8.3123**	8.4709	8.4173	8.4515
Count	0	3	20	12	6	6

B.2 NEAREST CENTROID CLASSFICATION

Table 4: UCR nearest centroid classification accuracy

Dataset	**subgradient**	**DBA**	**soft-DTW**	**ns-DTW (g_1)**	**ns-DTW (g_2)**	**ns-DTW (g_3)**
Adiac	0.4490	0.4388	0.6224	0.6327	**0.65**	0.6327
ArrowHead	0.1111	0.2222	**0.33**	0.2222	**0.33**	0.1111
Beef	0.2500	0.2500	0.2500	0.1250	**0.38**	0.2500
BeetleFly	0.8000	**1.00**	**1.00**	**1.00**	0.8000	0.8000
BirdChicken	0.8000	0.8000	0.8000	**1.00**	0.8000	**1.00**
CBF	0.8750	**1.00**	**1.00**	**1.00**	0.8750	0.8750
Car	0.6000	0.5333	**0.73**	0.6667	0.6667	0.6667
ChlorineConcentration	0.2735	0.3504	**0.38**	0.3675	0.3162	0.3419
CinCECGTorso	0.3000	0.4000	0.4000	0.3000	0.3000	**0.50**
Coffee	0.0000	0.0000	0.0000	**0.14**	0.0000	0.0000
Computers	0.6349	**0.75**	0.7143	0.6667	0.6825	0.6508
CricketX	0.3878	0.4592	0.4694	0.5204	**0.62**	0.5918
CricketY	0.3878	0.4490	0.4694	0.4796	0.5102	**0.53**
CricketZ	0.3980	0.5408	0.5816	0.5612	0.5510	**0.65**
DistalPhalanxOutlineAgeGroup	0.8700	0.7900	0.7900	0.8100	**0.91**	0.8200
DistalPhalanxOutlineCorrect	0.1000	0.0867	0.0933	0.1067	**0.19**	0.1400
DistalPhalanxTW	**0.04**	0.0000	0.0000	0.0000	0.0100	0.0100
ECG200	0.1200	0.0800	0.0800	0.0800	**0.28**	0.0000
ECGFiveDays	0.5000	0.5000	0.1667	0.1667	**0.67**	**0.67**
Earthquakes	0.0494	**0.07**	**0.07**	0.0617	0.0370	0.0617
FaceAll	0.8357	0.8429	0.8714	0.9000	**0.93**	**0.93**
FacesUCR	**0.90**	0.7800	0.8600	0.8600	0.8800	**0.90**
GunPoint	0.3846	**0.77**	0.6923	0.6154	0.6923	0.6154
Ham	0.6429	0.6071	0.7143	**0.79**	0.6429	0.6429
MedicalImages	0.4583	0.4479	0.4479	0.4375	0.4271	**0.52**
MiddlePhalanxOutlineAgeGroup	0.7600	**0.81**	**0.81**	**0.81**	0.7600	0.7700
MiddlePhalanxOutlineCorrect	0.2467	0.2067	0.2333	0.2800	0.2267	**0.39**
MiddlePhalanxTW	0.0300	0.0200	0.0300	0.0100	0.0300	**0.07**
MoteStrain	0.6000	0.8000	0.8000	0.8000	**1.00**	0.6000
ProximalPhalanxTW	**0.07**	0.0100	0.0100	0.0000	0.0000	0.0000
RefrigerationDevices	**0.61**	0.4787	0.4787	0.5000	0.5638	0.5106
ScreenType	0.4255	0.4149	0.4787	**0.51**	0.3936	0.3936
ShapeletSim	0.2000	0.4000	0.2000	0.4000	**0.60**	0.2000
ShapesAll	0.5333	0.6600	0.6533	**0.67**	0.6600	0.6067
SmallKitchenAppliances	0.6277	0.6064	0.6170	**0.64**	0.6064	0.5957
SonyAIBORobotSurface1	**1.00**	0.6000	0.6000	0.6000	**1.00**	0.6000
SonyAIBORobotSurface2	0.8571	**1.00**	**1.00**	0.8571	0.7143	0.5714
SyntheticControl	**1.00**	0.9867	**1.00**	0.9867	**1.00**	**1.00**
Trace	0.8800	0.8800	0.9200	0.9200	**1.00**	0.9600
TwoLeadECG	0.6667	0.8333	0.8333	**1.00**	0.8333	0.8333
Wine	0.5333	0.3333	0.3333	0.4667	0.5333	**0.67**
Worms	0.4565	0.4348	0.4783	**0.50**	0.3478	0.4783
WormsTwoClass	0.5870	0.6739	0.6739	0.6739	0.6522	**0.70**
Count	6	7	9	11	14	13

B.3 1NN Classification

Table 5: UCR 1-nearest neighbor classification accuracy

Dataset	**DBA**	**soft-DTW**	**ns-DTW (g_1)**	**ns-DTW (g_2)**	**ns-DTW (g_3)**
Adiac	0.5204	0.5714	**0.62**	0.5714	0.5510
ArrowHead	**0.89**	**0.89**	0.6667	0.7778	**0.89**
Beef	0.2500	0.2500	**0.62**	0.5000	0.2500
BeetleFly	0.8000	0.8000	0.8000	**1.00**	0.8000
BirdChicken	0.6000	0.6000	**1.00**	**1.00**	0.6000
CBF	**1.00**	**1.00**	**1.00**	**1.00**	**1.00**
Car	0.3333	0.5333	**0.67**	0.4667	0.6000
ChlorineConcentration	0.4359	0.4872	0.4701	**0.56**	0.4957
CinCECGTorso	0.5000	0.5000	0.6000	**0.70**	0.5000
Coffee	**1.00**	**1.00**	**1.00**	**1.00**	**1.00**
Computers	**0.76**	**0.76**	0.5556	0.7460	**0.76**
CricketX	0.7449	**0.79**	0.7245	0.7449	**0.79**
CricketY	0.6735	0.6837	0.7041	**0.72**	0.7041
CricketZ	0.7347	0.7347	0.6735	0.7143	**0.74**
DistalPhalanxOutlineAgeGroup	0.7700	0.7700	**0.81**	0.7800	0.7700
DistalPhalanxOutlineCorrect	0.7733	0.7733	**0.81**	0.8000	0.7667
DistalPhalanxTW	0.7200	**0.75**	0.6900	0.7300	0.7400
ECG200	0.7600	0.7600	0.7200	**0.88**	0.7600
ECGFiveDays	0.8333	**1.00**	0.6667	0.5000	**1.00**
Earthquakes	0.7654	0.7654	**0.78**	0.7407	0.7654
FaceAll	0.9214	0.9500	0.9214	0.9357	**0.96**
FacesUCR	0.7600	**0.78**	0.6667	0.6667	**0.78**
GunPoint	0.8462	**0.92**	0.8600	0.9200	**0.92**
Ham	0.7500	0.7500	**0.92**	0.7692	0.8214
MedicalImages	0.7083	0.7604	**0.82**	0.7857	0.7083
MiddlePhalanxOutlineAgeGroup	0.7000	0.6900	0.6979	0.6979	**0.73**
MiddlePhalanxOutlineCorrect	0.7267	0.7733	**0.85**	0.8000	0.7667
MiddlePhalanxTW	0.6200	0.5900	0.7400	**0.79**	0.6000
MoteStrain	**0.80**	**0.80**	0.5900	0.5500	**0.80**
ProximalPhalanxTW	0.7500	0.7500	0.6000	**0.80**	0.7600
RefrigerationDevices	0.5957	0.6383	0.7100	**0.83**	0.6383
ScreenType	0.4574	0.5106	**0.70**	0.6702	0.4574
ShapeletSim	0.2000	0.2000	0.4787	**0.52**	0.2000
ShapesAll	0.7067	0.7467	0.6000	0.4000	**0.75**
SmallKitchenAppliances	0.6596	0.6915	0.7267	**0.79**	0.6702
SonyAIBORobotSurface1	**0.80**	**0.80**	0.5851	0.6383	**0.80**
SonyAIBORobotSurface2	**0.86**	**0.86**	0.8000	0.8000	**0.86**
SyntheticControl	**1.00**	**1.00**	0.8571	0.7143	**1.00**
Trace	**1.00**	**1.00**	**1.00**	**1.00**	**1.00**
TwoLeadECG	**1.00**	**1.00**	0.9600	**1.00**	**1.00**
Wine	**0.87**	**0.87**	0.8333	0.6667	**0.87**
Worms	0.4565	0.4565	0.6667	**0.87**	0.4565
WormsTwoClass	0.7391	**0.76**	0.4348	0.5000	0.7391
Count	11	17	14	16	19

B.4 Clustering

Table 6: UCR Clustering DTW Losses

Dataset	DBA	soft-DTW	ns-DTW (g_1)	ns-DTW (g_2)	ns-DTW (g_3)
Adiac	0.0921	**0.0878**	0.0885	0.0882	0.0885
ArrowHead	1.2090	1.0741	1.0624	**1.0433**	1.0650
Beef	2.8558	2.2851	**2.1169**	2.1680	2.1365
BeetleFly	20.6455	19.8514	19.0531	**18.9430**	19.0679
BirdChicken	9.4679	**7.9387**	8.0163	8.0368	8.0304
CBF	12.0459	11.8482	11.8576	11.7534	**11.7463**
Car	0.8623	0.6263	0.5699	**0.5669**	0.5676
ChlorineConcentration	6.5869	6.4396	6.4328	6.4346	**6.4263**
CinCECGTorso	**669.7685**	**669.7685**	**669.7685**	**669.7685**	**669.7685**
Coffee	0.4366	**0.4297**	0.4305	0.4304	0.4306
Computers	143.5164	141.2816	**137.3022**	141.0881	139.3186
CricketX	**114.1204**	**114.1204**	**114.1204**	**114.1204**	**114.1204**
CricketY	**103.0182**	**103.0182**	**103.0182**	**103.0182**	**103.0182**
CricketZ	**124.6247**	**124.6247**	**124.6247**	**124.6247**	**124.6247**
DiatomSizeReduction	0.0712	0.0756	**0.0628**	0.0632	0.0633
DistalPhalanxOutlineAgeGroup	0.3678	**0.3633**	0.3636	0.3637	0.3637
DistalPhalanxOutlineCorrect	0.8450	**0.7544**	0.7631	0.7635	0.7645
DistalPhalanxTW	0.3325	0.3319	0.3303	**0.3292**	0.3305
ECG200	4.5978	**4.5201**	4.5334	4.5394	4.5334
ECG5000	6.4048	6.6103	6.5432	**6.4040**	6.5932
ECGFiveDays	5.7908	5.6721	**5.5425**	5.5447	5.6063
Earthquakes	**437.7200**	**437.7200**	**437.7200**	**437.7200**	**437.7200**
FaceAll	**34.8896**	**34.8896**	**34.8896**	**34.8896**	**34.8896**
FaceFour	21.2485	20.2836	20.1979	**20.1897**	20.2069
FacesUCR	**27.0649**	**27.0649**	**27.0649**	**27.0649**	**27.0649**
GunPoint	1.1022	1.0099	0.9990	**0.9987**	0.9989
Ham	17.1259	17.0784	17.0572	**17.0463**	17.0749
MedicalImages	4.1345	3.5272	3.4652	3.4744	**3.4197**
MiddlePhalanxOutlineAgeGroup	0.2368	**0.2329**	0.2338	0.2335	0.2338
MiddlePhalanxOutlineCorrect	0.3350	**0.3348**	0.3348	0.3348	0.3348
MiddlePhalanxTW	0.2193	**0.2134**	0.2171	0.2152	0.2172
MoteStrain	18.8957	19.0558	19.0490	19.0497	**18.8197**
ProximalPhalanxTW	0.1591	0.1584	0.1585	**0.1584**	0.1585
RefrigerationDevices	122.9185	115.9638	**113.0523**	116.9189	114.3597
ScreenType	108.5347	104.8087	104.5366	**103.5914**	104.1625
ShapeletSim	127.3930	122.4791	120.5546	120.9429	**120.4151**
ShapesAll	**25.5056**	25.5057	**25.5056**	**25.5056**	**25.5056**
SmallKitchenAppliances	123.9963	123.7793	**122.3944**	123.1039	123.3957
SonyAIBORobotSurface1	4.9519	4.7078	4.6157	**4.6127**	4.6157
SonyAIBORobotSurface2	8.9998	8.8919	8.8860	8.8879	**8.8808**
SyntheticControl	8.7978	8.7625	**8.6648**	8.6736	8.6778
Trace	3.5626	3.4207	**2.9248**	2.9365	2.9483
TwoLeadECG	0.9103	**0.8642**	0.8644	0.8645	0.8644
Wine	0.0697	**0.0649**	0.0702	0.0691	0.0678
WordSynonyms	**27.5408**	**27.5408**	**27.5408**	**27.5408**	**27.5408**
Worms	**451.2960**	**451.2960**	**451.2960**	**451.2960**	**451.2960**
WormsTwoClass	81.4757	78.6740	**76.7911**	78.2881	78.3617
Count	10	20	19	21	16

C Ablation Study of Averaging

Table 7: Ablation Study of Averaging (Grouping g_1): Comparison of UCR Barycenter DTW Losses across different parameters τ. Bold indicates the lowest loss.

Dataset	**ns-DTW (g_1)**			
	$\tau = \mathbf{0.95}$	$\tau = \mathbf{0.90}$	$\tau = \mathbf{0.85}$	$\tau = \mathbf{0.80}$
Adiac	0.2551	0.2550	0.2549	**0.2549**
ArrowHead	1.1772	**1.1771**	1.1772	1.1774
Beef	**4.1005**	4.1014	4.1068	4.1015
BeetleFly	**4.3015**	4.3096	4.3031	4.3037
BirdChicken	2.4647	2.4646	2.4649	**2.4575**
CBF	**3.7857**	**3.7857**	**3.7857**	**3.7857**
Car	**0.6489**	0.6493	0.6577	0.6575
ChlorineConcentration	**3.4750**	**3.4750**	**3.4750**	3.4750
CinCECGTorso	8.3677	8.5311	**8.3574**	8.5775
Coffee	0.5890	0.5890	0.5889	**0.5889**
Computers	14.6314	14.6176	14.6282	**14.6000**
CricketX	5.8424	5.8500	**5.8272**	5.8537
CricketY	**5.5948**	5.5975	5.5974	5.5950
CricketZ	5.3866	5.3843	5.3875	**5.3840**
DiatomSizeReduction	**0.2278**	0.2278	0.2291	0.2289
DistalPhalanxOutlineAgeGroup	**0.7059**	**0.7059**	**0.7059**	**0.7059**
DistalPhalanxOutlineCorrect	**0.6666**	**0.6666**	**0.6666**	**0.6666**
DistalPhalanxTW	**0.3458**	**0.3458**	**0.3458**	**0.3458**
ECG200	2.6704	2.6704	2.6703	**2.6703**
ECG5000	**2.2057**	2.2060	2.2063	**2.2057**
ECGFiveDays	2.5275	**2.4832**	2.5278	2.5324
Earthquakes	**10.8445**	10.8446	10.8446	10.8446
FaceAll	**3.0059**	3.0109	3.0110	3.0104
FaceFour	**5.3563**	**5.3563**	**5.3563**	**5.3563**
FacesUCR	**3.2074**	**3.2074**	**3.2074**	**3.2074**
GunPoint	1.7460	1.7440	**1.7202**	1.7458
Ham	**4.0997**	4.1004	4.1003	4.1019
MedicalImages	2.6887	2.6888	2.6887	**2.6886**
MiddlePhalanxOutlineAgeGroup	**0.5152**	**0.5152**	**0.5152**	**0.5152**
MiddlePhalanxOutlineCorrect	**0.6389**	**0.6389**	**0.6389**	**0.6389**
MiddlePhalanxTW	**0.3282**	0.3282	0.3282	0.3282
MoteStrain	4.2600	**4.2588**	4.2589	4.2589
ProximalPhalanxTW	**0.3390**	0.3398	0.3396	0.3395
RefrigerationDevices	8.2907	**8.2763**	8.3036	8.3232
ScreenType	12.0787	12.0795	12.1121	**12.0785**
ShapeletSim	11.0850	**11.0820**	11.1077	11.1077
ShapesAll	1.0652	1.0652	**1.0638**	1.0657
SmallKitchenAppliances	9.9110	9.9131	**9.3478**	9.3585
SonyAIBORobotSurface1	**1.6774**	**1.6774**	**1.6774**	**1.6774**
SonyAIBORobotSurface2	**2.5914**	**2.5914**	**2.5914**	**2.5914**
SyntheticControl	**4.1615**	**4.1615**	**4.1615**	**4.1615**
Trace	0.8954	**0.8949**	0.8969	0.8962
TwoLeadECG	0.8555	0.8554	0.8554	**0.8553**
Wine	**0.3245**	0.3245	0.3245	0.3245
WordSynonyms	2.1832	**2.1731**	2.1836	2.1744
Worms	**10.2557**	10.4207	10.4068	10.4219
WormsTwoClass	8.4709	**8.4596**	8.4805	8.4603
Count	25	20	17	21

Table 8: Ablation Study of Averaging (Grouping g_2): Comparison of UCR Barycenter DTW Losses across different parameters τ. Bold indicates the lowest loss.

Dataset	**ns-DTW (g_2)**			
	$\tau = \mathbf{0.95}$	$\tau = \mathbf{0.90}$	$\tau = \mathbf{0.85}$	$\tau = \mathbf{0.80}$
Adiac	0.2553	0.2553	0.2553	**0.2552**
ArrowHead	1.1663	**1.1651**	1.1652	1.1846
Beef	4.1025	4.1114	4.1036	**4.0924**
BeetleFly	4.3052	4.3067	4.3170	**4.3045**
BirdChicken	2.4589	2.4597	**2.4540**	2.4633
CBF	3.8330	**3.8132**	**3.8132**	3.8140
Car	**0.6492**	0.6493	0.6571	0.6576
ChlorineConcentration	3.4750	3.4750	**3.4749**	3.4750
CinCECGTorso	**8.3597**	8.4085	8.5551	8.4076
Coffee	**0.5892**	0.5894	0.5906	0.5901
Computers	14.6228	14.6119	14.6227	**14.6075**
CricketX	5.8423	**5.8244**	5.8738	5.8396
CricketY	**5.5944**	5.5968	5.5980	5.5974
CricketZ	5.3852	5.3829	5.3826	**5.3826**
DiatomSizeReduction	0.2278	0.2275	0.2274	**0.2271**
DistalPhalanxOutlineAgeGroup	0.7059	**0.7058**	0.7059	0.7058
DistalPhalanxOutlineCorrect	**0.6666**	**0.6666**	**0.6666**	**0.6666**
DistalPhalanxTW	**0.3458**	0.3458	0.3458	0.3459
ECG200	2.6726	**2.6718**	2.6738	2.6720
ECG5000	2.2080	2.2074	2.2065	**2.2011**
ECGFiveDays	**2.5185**	2.5265	2.5293	2.5237
Earthquakes	**10.8293**	10.8420	10.8365	10.8365
FaceAll	3.0224	3.0080	**3.0065**	3.0178
FaceFour	**5.3563**	5.3564	5.3564	5.3565
GunPoint	1.7464	**1.7436**	1.7441	1.7451
Ham	4.0929	**4.0802**	4.1005	4.1018
MedicalImages	**2.6858**	2.6864	2.6860	2.6870
MiddlePhalanxOutlineAgeGroup	0.5145	**0.5142**	0.5143	0.5143
MiddlePhalanxOutlineCorrect	0.6389	0.6389	**0.6388**	0.6388
MiddlePhalanxTW	**0.3282**	0.3282	0.3282	0.3282
MoteStrain	4.2591	4.2565	**4.2546**	4.2567
ProximalPhalanxTW	0.3399	**0.3397**	0.3399	0.3399
RefrigerationDevices	8.9489	8.9519	8.9514	**8.8522**
ScreenType	12.0857	12.0816	**12.0815**	12.0838
ShapeletSim	**11.0833**	11.0836	11.1077	11.1078
ShapesAll	**1.0653**	1.0740	1.0662	1.0680
SmallKitchenAppliances	9.4743	**9.4160**	9.4293	9.9123
SonyAIBORobotSurface1	**1.6774**	**1.6774**	**1.6774**	**1.6774**
SonyAIBORobotSurface2	**2.5914**	**2.5914**	**2.5914**	**2.5914**
SyntheticControl	4.1615	4.1615	4.1615	**4.1615**
Trace	**0.8949**	0.9133	0.8964	0.9030
TwoLeadECG	0.8554	0.8549	0.8551	**0.8547**
Wine	**0.3251**	0.3253	0.3264	0.3260
Worms	10.4246	**10.4022**	10.4252	10.4123
WormsTwoClass	8.5204	**8.4643**	8.4992	8.5186
Count	17	15	10	13

Table 9: Ablation Study of Averaging (Grouping g_3): Comparison of UCR Barycenter DTW Losses across different parameters τ. Bold indicates the lowest loss.

Dataset	ns-DTW (g_3)			
	$\tau = \mathbf{0.95}$	$\tau = \mathbf{0.90}$	$\tau = \mathbf{0.85}$	$\tau = \mathbf{0.80}$
Adiac	**0.2552**	0.2553	0.2554	0.2556
ArrowHead	**1.1643**	1.1774	1.1789	1.1775
Beef	**4.1015**	4.1018	4.1054	4.1238
BeetleFly	**4.3045**	4.3085	4.3055	4.3070
BirdChicken	2.4642	2.4654	2.4548	**2.4548**
CBF	3.8332	3.8331	**3.8132**	3.8140
Car	0.6489	0.6486	**0.6446**	0.6485
ChlorineConcentration	3.4751	3.4746	**3.4745**	3.4746
CinCECGTorso	**8.3599**	8.5016	8.3633	8.5583
Coffee	**0.5893**	0.5903	0.5904	0.5905
Computers	14.6203	**14.6059**	14.6578	14.6558
CricketX	5.8534	5.9529	**5.8229**	6.0129
CricketY	5.5951	5.5954	**5.5947**	5.5952
CricketZ	5.3862	5.3891	5.3829	**5.3817**
DiatomSizeReduction	**0.2278**	0.2280	0.2285	0.2279
DistalPhalanxOutlineAgeGroup	0.7057	0.7060	0.7055	**0.7047**
DistalPhalanxOutlineCorrect	**0.6666**	**0.6666**	**0.6666**	**0.6666**
DistalPhalanxTW	0.3458	0.3459	0.3458	**0.3458**
ECG200	2.6704	2.6704	**2.6704**	**2.6704**
ECG5000	2.2060	2.2061	2.2056	**2.2000**
ECGFiveDays	2.5252	2.5248	2.5262	**2.4842**
Earthquakes	**10.8283**	10.8446	10.8447	10.8446
FaceAll	3.0104	3.0102	3.0108	**3.0096**
FaceFour	**5.3562**	5.3562	5.3562	5.3562
FacesUCR	**3.2074**	**3.2074**	**3.2074**	**3.2074**
GunPoint	**1.7408**	1.7427	1.7440	1.7423
Ham	**4.0984**	4.0993	4.0993	4.1070
MedicalImages	2.6887	2.6896	2.6896	**2.6886**
MiddlePhalanxOutlineAgeGroup	0.5143	0.5141	**0.5141**	**0.5141**
MiddlePhalanxOutlineCorrect	**0.6389**	0.6390	0.6390	0.6390
MiddlePhalanxTW	**0.3281**	**0.3281**	**0.3281**	**0.3281**
MoteStrain	4.2582	**4.2565**	4.2572	4.2571
ProximalPhalanxTW	0.3399	0.3400	0.3398	**0.3397**
RefrigerationDevices	**8.8975**	8.9557	8.9514	8.9532
ScreenType	**12.0816**	12.0858	12.0848	12.0858
ShapeletSim	**11.0834**	11.1077	11.1077	11.1077
ShapesAll	1.0690	1.0688	1.0683	**1.0641**
SmallKitchenAppliances	9.4851	**9.3029**	9.7840	9.7895
SonyAIBORobotSurface1	1.6774	1.6773	**1.6773**	**1.6773**
SonyAIBORobotSurface2	**2.5914**	**2.5914**	2.5914	2.5914
SyntheticControl	**4.1615**	**4.1615**	**4.1615**	**4.1615**
Trace	0.8970	0.8961	0.9118	**0.8960**
TwoLeadECG	0.8554	0.8554	0.8553	**0.8553**
Wine	0.3240	**0.3238**	0.3242	0.3240
WordSynonyms	2.1858	**2.1513**	2.1593	2.1863
Worms	10.4158	**10.2059**	10.4138	10.4293
WormsTwoClass	8.4515	8.4789	8.4532	**8.4484**
Count	20	11	12	20

D Ablation Study of Classification

Table 10: Ablation Study of Classification (Grouping g_1): Comparison of nearest centroid classification accuracy across different parameters τ. Bold indicates the highest accuracy.

Dataset	**ns-DTW (g_1)**			
	$\tau = \mathbf{0.95}$	$\tau = \mathbf{0.90}$	$\tau = \mathbf{0.85}$	$\tau = \mathbf{0.80}$
Adiac	**0.63**	0.5306	0.5918	0.5408
ArrowHead	0.2222	0.2222	**0.33**	0.2222
Beef	0.1250	**0.50**	0.2500	0.3750
BeetleFly	**1.00**	0.8000	0.8000	0.8000
BirdChicken	**1.00**	0.6000	0.6000	0.6000
CBF	**1.00**	**1.00**	0.8750	**1.00**
Car	0.6667	0.7333	0.7333	**0.80**
ChlorineConcentration	**0.37**	0.3162	0.2137	0.3504
CinCECGTorso	0.3000	0.5000	**0.60**	0.3000
Coffee	**0.14**	0.0000	0.0000	**0.14**
Computers	0.6667	0.5397	**0.68**	0.5714
CricketX	0.5204	0.6122	0.5000	**0.63**
CricketY	0.4796	0.5612	0.4490	**0.57**
CricketZ	0.5612	0.5816	0.5408	**0.59**
DistalPhalanxOutlineAgeGroup	0.8100	0.8400	0.8300	**0.85**
DistalPhalanxOutlineCorrect	0.1067	0.2200	**0.23**	0.0867
DistalPhalanxTW	0.0000	0.0200	0.0300	**0.06**
ECG200	0.0800	0.1600	0.1600	**0.28**
ECGFiveDays	0.1667	**0.67**	0.5000	0.5000
Earthquakes	**0.06**	0.0123	0.0123	**0.06**
FaceAll	0.9000	**0.92**	0.9143	0.9143
FacesUCR	**0.86**	**0.86**	**0.86**	0.8000
GunPoint	0.6154	0.6154	0.6154	**0.85**
Ham	**0.79**	0.6429	0.7500	0.6429
MedicalImages	0.4375	0.4271	**0.47**	**0.47**
MiddlePhalanxOutlineAgeGroup	**0.81**	0.7300	0.7700	0.8000
MiddlePhalanxOutlineCorrect	**0.28**	0.2533	0.2267	0.2067
MiddlePhalanxTW	0.0100	**0.05**	**0.05**	**0.05**
MoteStrain	**0.80**	**0.80**	**0.80**	**0.80**
ProximalPhalanxTW	**0.00**	**0.00**	**0.00**	**0.00**
RefrigerationDevices	0.5000	0.5426	**0.60**	0.5106
ScreenType	**0.51**	0.4149	0.4043	0.4574
ShapeletSim	**0.40**	0.0000	0.2000	**0.40**
ShapesAll	**0.67**	0.6133	0.6600	0.6600
SmallKitchenAppliances	**0.64**	0.5745	0.5745	**0.64**
SonyAIBORobotSurface1	0.6000	**1.00**	0.8000	**1.00**
SonyAIBORobotSurface2	0.8571	0.8571	0.5714	**1.00**
SyntheticControl	0.9867	**1.00**	**1.00**	**1.00**
Trace	0.9200	**1.00**	0.8400	**1.00**
TwoLeadECG	**1.00**	0.6667	0.6667	0.8333
Wine	0.4667	0.3333	**0.73**	0.4667
Worms	**0.50**	0.2826	0.3913	0.4130
WormsTwoClass	**0.67**	0.5652	0.5435	0.5652
Count	20	11	12	21

Table 11: Ablation Study of Classification (Grouping g_2): Comparison of nearest centroid classification accuracy across different parameters τ. Bold indicates the highest accuracy.

Dataset	**ns-DTW (g_2)**			
	$\tau = \mathbf{0.95}$	$\tau = \mathbf{0.90}$	$\tau = \mathbf{0.85}$	$\tau = \mathbf{0.80}$
Adiac	**0.65**	0.5510	0.6122	0.5714
ArrowHead	**0.33**	0.1111	0.0000	0.1111
Beef	0.3750	**0.50**	**0.50**	0.3750
BeetleFly	**0.80**	**0.80**	0.6000	0.6000
BirdChicken	0.8000	**1.00**	0.8000	0.8000
CBF	**0.88**	**0.88**	**0.88**	**0.88**
Car	**0.67**	**0.67**	**0.67**	**0.67**
ChlorineConcentration	0.3162	0.2906	0.3675	**0.38**
CinCECGTorso	0.3000	0.3000	0.4000	**0.50**
Coffee	**0.00**	**0.00**	**0.00**	**0.00**
Computers	**0.68**	0.6508	0.6508	0.6349
CricketX	0.6224	0.5204	0.5714	**0.65**
CricketY	0.5102	**0.61**	0.5612	0.5918
CricketZ	0.5510	**0.61**	0.4592	0.4796
DistalPhalanxOutlineAgeGroup	**0.91**	0.8500	0.8800	0.8400
DistalPhalanxOutlineCorrect	0.1867	0.1400	0.1667	**0.29**
DistalPhalanxTW	0.0100	0.0100	0.0000	**0.02**
ECG200	**0.28**	0.2400	0.2000	0.1200
ECGFiveDays	0.6667	0.5000	0.6667	**0.83**
Earthquakes	0.0370	0.0247	**0.05**	0.0370
FaceAll	**0.93**	0.9143	0.8643	0.9000
FacesUCR	0.8800	**0.94**	0.8200	0.9000
GunPoint	**0.69**	**0.69**	0.6154	**0.69**
Ham	0.6429	0.6071	0.7500	**0.86**
MedicalImages	0.4271	0.4271	0.3646	**0.49**
MiddlePhalanxOutlineAgeGroup	0.7600	**0.78**	0.7500	0.7500
MiddlePhalanxOutlineCorrect	0.2267	0.2600	0.3600	**0.41**
MiddlePhalanxTW	0.0300	0.0500	**0.07**	0.0600
MoteStrain	**1.00**	0.8000	0.8000	0.6000
ProximalPhalanxTW	0.0000	**0.01**	0.0000	0.0000
RefrigerationDevices	0.5638	**0.68**	0.5426	0.5426
ScreenType	0.3936	**0.48**	0.4149	0.4255
ShapeletSim	**0.60**	0.2000	0.2000	0.4000
ShapesAll	0.6600	0.6533	0.6467	**0.68**
SmallKitchenAppliances	0.6064	**0.73**	0.6383	0.5957
SonyAIBORobotSurface1	**1.00**	0.8000	**1.00**	**1.00**
SonyAIBORobotSurface2	0.7143	0.7143	**1.00**	**1.00**
SyntheticControl	**1.00**	0.9867	**1.00**	0.9867
Trace	**1.00**	**1.00**	0.9600	**1.00**
TwoLeadECG	**0.83**	0.6667	0.6667	0.6667
Wine	**0.53**	**0.53**	**0.53**	0.2667
Worms	0.3478	0.5000	0.3696	**0.52**
WormsTwoClass	0.6522	0.5217	**0.67**	0.6087
Count	18	17	11	18

Table 12: Ablation Study of Classification (Grouping g_3): Comparison of nearest centroid classification accuracy across different parameters τ. Bold indicates the highest accuracy.

Dataset	**ns-DTW (g_3)**			
	$\tau = \mathbf{0.95}$	$\tau = \mathbf{0.90}$	$\tau = \mathbf{0.85}$	$\tau = \mathbf{0.80}$
Adiac	**0.63**	0.6020	0.5918	0.6020
ArrowHead	0.1111	**0.33**	**0.33**	0.2222
Beef	**0.25**	0.1250	0.1250	**0.25**
BeetleFly	**0.80**	0.6000	0.6000	**0.80**
BirdChicken	**1.00**	0.6000	0.4000	0.8000
CBF	0.8750	**1.00**	0.8750	0.8750
Car	0.6667	**0.80**	0.7333	**0.80**
ChlorineConcentration	**0.34**	0.2564	0.3077	0.3333
CinCECGTorso	**0.50**	**0.50**	0.4000	0.2000
Coffee	0.0000	0.0000	0.0000	**0.14**
Computers	**0.65**	**0.65**	0.5873	0.6190
CricketX	**0.59**	0.5612	0.5612	0.5510
CricketY	0.5306	0.5102	**0.56**	0.5408
CricketZ	**0.65**	0.5306	0.5000	0.5204
DistalPhalanxOutlineAgeGroup	0.8200	**0.86**	0.8100	0.8500
DistalPhalanxOutlineCorrect	0.1400	**0.26**	0.0867	0.1933
DistalPhalanxTW	0.0100	**0.03**	0.0100	0.0200
ECG200	0.0000	**0.20**	0.1200	0.1200
ECGFiveDays	0.6667	0.5000	**1.00**	0.6667
Earthquakes	**0.06**	0.0247	0.0247	0.0247
FaceAll	**0.93**	0.9143	0.9143	0.8857
FacesUCR	0.9000	0.7600	0.9200	**0.94**
GunPoint	0.6154	**0.77**	**0.77**	0.4615
Ham	0.6429	0.7143	**0.75**	**0.75**
MedicalImages	**0.52**	0.4271	0.3542	0.3542
MiddlePhalanxOutlineAgeGroup	0.7700	0.7500	**0.80**	0.7900
MiddlePhalanxOutlineCorrect	0.3867	0.3667	**0.43**	0.2867
MiddlePhalanxTW	**0.07**	0.0600	0.0400	0.0400
MoteStrain	0.6000	**0.80**	0.6000	**0.80**
ProximalPhalanxTW	**0.00**	**0.00**	**0.00**	**0.00**
RefrigerationDevices	0.5106	0.5426	**0.61**	0.5319
ScreenType	0.3936	**0.44**	0.4255	0.4149
ShapeletSim	0.2000	**0.40**	0.2000	**0.40**
ShapesAll	0.6067	0.6467	**0.72**	0.6533
SmallKitchenAppliances	0.5957	**0.66**	0.6489	0.6277
SonyAIBORobotSurface1	0.6000	0.8000	**1.00**	0.8000
SonyAIBORobotSurface2	0.5714	**1.00**	**1.00**	0.7143
SyntheticControl	**1.00**	**1.00**	0.9867	0.9867
Trace	**0.96**	**0.96**	0.9200	**0.96**
TwoLeadECG	0.8333	0.8333	0.3333	**1.00**
Wine	**0.67**	0.5333	0.4667	0.4000
Worms	**0.48**	0.4348	0.4130	0.3696
WormsTwoClass	**0.70**	0.6522	0.6304	0.5870
Count	19	18	12	11

E Ablation Study for Clustering

Table 13: Ablation Study of Clustering (Grouping g_1): Comparison of UCR Clustering DTW Losses across different parameters τ. Bold indicates the lowest loss.

Dataset	ns-DTW (g_1)			
	$\tau = \mathbf{0.95}$	$\tau = \mathbf{0.90}$	$\tau = \mathbf{0.85}$	$\tau = \mathbf{0.80}$
Adiac	0.0933	0.0887	0.0887	**0.0885**
ArrowHead	**1.0624**	1.0781	1.0750	1.0723
Beef	2.6543	2.3194	**2.1169**	2.6488
BeetleFly	**19.0531**	19.0865	19.0850	19.1989
BirdChicken	**8.0163**	8.1141	8.0221	8.0705
CBF	11.9793	11.8627	**11.8576**	11.8919
Car	0.5828	0.6079	**0.5699**	0.5820
ChlorineConcentration	**6.4328**	6.4504	6.4373	6.4452
CinCECGTorso	**669.7685**	**669.7685**	**669.7685**	**669.7685**
Coffee	0.4340	0.4313	0.4305	**0.4305**
Computers	141.2125	142.1296	142.4221	**137.3022**
CricketX	**114.1204**	**114.1204**	**114.1204**	**114.1204**
CricketY	**103.0182**	**103.0182**	**103.0182**	**103.0182**
CricketZ	**124.6247**	**124.6247**	**124.6247**	**124.6247**
DiatomSizeReduction	0.1008	0.0634	0.0631	**0.0628**
DistalPhalanxOutlineAgeGroup	**0.3636**	0.3646	0.3639	0.3639
DistalPhalanxOutlineCorrect	0.7662	**0.7631**	0.7662	0.7644
DistalPhalanxTW	0.3305	0.3318	0.3305	**0.3303**
ECG200	4.5388	4.5473	**4.5334**	4.5376
ECG5000	6.7068	6.6826	6.5888	**6.5432**
ECGFiveDays	5.7248	**5.5425**	5.5456	5.6963
Earthquakes	**437.7200**	**437.7200**	**437.7200**	**437.7200**
FaceAll	34.8896	**34.8896**	**34.8896**	**34.8896**
FaceFour	20.2089	20.2031	**20.1979**	20.3103
FacesUCR	**27.0649**	**27.0649**	**27.0649**	**27.0649**
GunPoint	1.0274	**0.9990**	1.0012	1.0023
Ham	17.0643	17.0764	17.0641	**17.0572**
MedicalImages	**3.4652**	3.5714	3.5776	3.6044
MiddlePhalanxOutlineAgeGroup	**0.2338**	0.2349	0.2342	0.2340
MiddlePhalanxOutlineCorrect	0.3353	0.3349	0.3349	**0.3348**
MiddlePhalanxTW	**0.2171**	0.2180	0.2171	0.2178
MoteStrain	**19.0490**	19.0853	19.0503	19.0503
ProximalPhalanxTW	0.1595	0.1585	**0.1585**	0.1585
RefrigerationDevices	**113.0523**	114.4612	114.9686	117.9007
ScreenType	**104.5366**	105.8296	105.6790	104.8913
ShapeletSim	121.8188	120.5682	**120.5546**	120.7565
ShapesAll	25.5065	**25.5056**	**25.5056**	**25.5056**
SmallKitchenAppliances	124.1084	**122.3944**	123.6107	123.2592
SonyAIBORobotSurface1	**4.6157**	4.6442	4.6401	4.6435
SonyAIBORobotSurface2	8.8879	8.8915	8.8879	**8.8860**
SyntheticControl	**8.6648**	8.6900	8.6810	8.6787
Trace	2.9443	2.9413	2.9340	**2.9248**
TwoLeadECG	0.8646	0.8769	0.8648	**0.8644**
Wine	0.0704	0.0702	**0.0702**	0.0702
WordSynonyms	**27.5408**	**27.5408**	**27.5408**	**27.5408**
Worms	**451.2960**	**451.2960**	**451.2960**	**451.2960**
WormsTwoClass	78.2919	78.5687	**76.7911**	78.7067
Count	21	14	19	21

Table 14: Ablation Study of Clustering (Grouping g_2): Comparison of UCR Clustering DTW Losses across different parameters τ. Bold indicates the lowest loss.

Dataset	ns-DTW (g_2)			
	$\tau = \mathbf{0.95}$	$\tau = \mathbf{0.90}$	$\tau = \mathbf{0.85}$	$\tau = \mathbf{0.80}$
Adiac	0.0889	0.0886	**0.0882**	0.0887
ArrowHead	1.0626	1.0754	1.0447	**1.0433**
Beef	2.6517	2.6512	2.2552	**2.1680**
BeetleFly	19.1110	19.1173	**18.9430**	19.0810
BirdChicken	8.0838	**8.0368**	8.0901	8.0716
CBF	11.8548	11.8228	**11.7534**	11.8266
Car	**0.5669**	0.5728	0.5735	0.5785
ChlorineConcentration	**6.4346**	6.4438	6.4461	6.4400
CinCECGTorso	**669.7685**	**669.7685**	**669.7685**	**669.7685**
Coffee	0.4305	**0.4304**	0.4307	0.4314
Computers	143.9456	**141.0881**	142.3675	141.7750
CricketX	**114.1204**	**114.1204**	**114.1204**	**114.1204**
CricketY	**103.0182**	**103.0182**	**103.0182**	**103.0182**
CricketZ	**124.6247**	**124.6247**	**124.6247**	**124.6247**
DiatomSizeReduction	**0.0632**	0.0635	0.0633	0.0636
DistalPhalanxOutlineAgeGroup	0.3641	0.3640	**0.3637**	0.3639
DistalPhalanxOutlineCorrect	0.7654	0.7648	0.7641	**0.7635**
DistalPhalanxTW	0.3305	0.3305	0.3307	**0.3292**
ECG200	**4.5394**	4.5605	4.5595	4.5452
ECG5000	6.7502	6.5538	**6.4040**	6.5952
ECGFiveDays	5.6538	5.6400	5.5714	**5.5447**
Earthquakes	**437.7200**	**437.7200**	**437.7200**	**437.7200**
FaceAll	**34.8896**	**34.8896**	**34.8896**	**34.8896**
FaceFour	20.2089	20.2024	20.1946	**20.1897**
FacesUCR	**27.0649**	**27.0649**	**27.0649**	**27.0649**
GunPoint	**0.9987**	1.0007	1.0040	1.0036
Ham	17.0729	17.0593	**17.0463**	17.1152
MedicalImages	**3.4744**	3.5939	3.5652	3.5336
MiddlePhalanxOutlineAgeGroup	0.2336	**0.2335**	0.2337	0.2336
MiddlePhalanxOutlineCorrect	0.3349	0.3348	**0.3348**	0.3349
MiddlePhalanxTW	**0.2152**	0.2169	0.2169	0.2173
MoteStrain	**19.0497**	19.0506	19.0507	19.0507
ProximalPhalanxTW	**0.1584**	0.1584	0.1585	0.1586
RefrigerationDevices	119.7300	**116.9189**	119.4748	119.4159
ScreenType	104.6065	104.5283	**103.5914**	104.3206
ShapeletSim	121.4127	121.6850	122.1467	**120.9429**
ShapesAll	**25.5056**	**25.5056**	**25.5056**	**25.5056**
SmallKitchenAppliances	**123.1039**	123.6502	123.9712	124.0442
SonyAIBORobotSurface1	**4.6127**	4.6506	4.6475	4.6339
SonyAIBORobotSurface2	**8.8879**	8.8879	8.8879	8.8879
SyntheticControl	8.6874	8.6919	8.6829	**8.6736**
Trace	2.9486	2.9450	2.9467	**2.9365**
TwoLeadECG	0.8646	**0.8645**	0.8646	0.8652
Wine	0.0699	0.0694	0.0694	**0.0691**
WordSynonyms	**27.5408**	**27.5408**	**27.5408**	**27.5408**
Worms	**451.2960**	**451.2960**	**451.2960**	**451.2960**
WormsTwoClass	78.6962	**78.2881**	78.6430	78.4662
Count	22	17	18	20

Table 15: Ablation Study of Clustering (Grouping g_3): Comparison of UCR Clustering DTW Losses across different parameters τ. Bold indicates the lowest loss.

Dataset	**ns-DTW (g_3)**			
	$\tau = \mathbf{0.95}$	$\tau = \mathbf{0.90}$	$\tau = \mathbf{0.85}$	$\tau = \mathbf{0.80}$
Adiac	**0.0885**	0.0888	0.0888	0.0885
ArrowHead	**1.0650**	1.0663	1.0664	1.0665
Beef	2.2629	2.2551	2.2545	**2.1365**
BeetleFly	19.0952	19.0988	19.0856	**19.0679**
BirdChicken	8.0704	8.0366	**8.0304**	8.1060
CBF	11.7832	**11.7463**	11.8067	11.8216
Car	**0.5676**	0.5790	0.5970	0.5846
ChlorineConcentration	**6.4263**	6.4330	6.4319	6.4301
CinCECGTorso	**669.7685**	**669.7685**	**669.7685**	**669.7685**
Coffee	**0.4306**	0.4306	0.4307	0.4318
Computers	139.4716	140.3803	**139.3186**	142.6158
CricketX	**114.1204**	**114.1204**	**114.1204**	**114.1204**
CricketY	**103.0182**	**103.0182**	**103.0182**	**103.0182**
CricketZ	**124.6247**	**124.6247**	**124.6247**	**124.6247**
DiatomSizeReduction	0.0634	0.0634	**0.0633**	0.0635
DistalPhalanxOutlineAgeGroup	0.3640	0.3638	0.3640	**0.3637**
DistalPhalanxOutlineCorrect	0.7659	**0.7645**	0.7688	0.7692
DistalPhalanxTW	**0.3305**	0.3306	0.3318	0.3317
ECG200	4.5356	4.5382	**4.5334**	4.5380
ECG5000	6.6823	**6.5932**	6.7333	6.6061
ECGFiveDays	**5.6063**	5.6822	5.6325	5.7113
Earthquakes	**437.7200**	**437.7200**	**437.7200**	**437.7200**
FaceAll	**34.8896**	**34.8896**	**34.8896**	**34.8896**
FaceFour	20.2126	**20.2069**	20.2224	20.3481
FacesUCR	**27.0649**	**27.0649**	**27.0649**	**27.0649**
GunPoint	1.0012	**0.9989**	1.0012	0.9996
Ham	17.0756	17.1056	**17.0749**	17.1139
MedicalImages	**3.4197**	3.6215	3.5611	3.4369
MiddlePhalanxOutlineAgeGroup	0.2339	**0.2338**	0.2339	0.2339
MiddlePhalanxOutlineCorrect	0.3349	0.3348	0.3348	**0.3348**
MiddlePhalanxTW	**0.2172**	0.2174	0.2173	0.2173
MoteStrain	**18.8197**	19.0501	19.0500	19.0499
ProximalPhalanxTW	0.1585	**0.1585**	0.1586	0.1586
RefrigerationDevices	120.0953	**114.3597**	118.9731	115.0863
ScreenType	104.6496	104.7925	105.0297	**104.1625**
ShapeletSim	121.2170	120.8727	120.6381	**120.4151**
ShapesAll	**25.5056**	**25.5056**	**25.5056**	**25.5056**
SmallKitchenAppliances	123.8676	123.7506	**123.3957**	123.5583
SonyAIBORobotSurface1	4.6162	**4.6157**	4.6566	4.6330
SonyAIBORobotSurface2	8.8879	8.8856	8.8813	**8.8808**
SyntheticControl	8.6781	8.7188	**8.6778**	8.6984
Trace	2.9488	2.9490	2.9518	**2.9483**
TwoLeadECG	0.8646	0.8646	0.8646	**0.8644**
Wine	0.0686	0.0682	0.0680	**0.0678**
WordSynonyms	**27.5408**	**27.5408**	**27.5408**	**27.5408**
Worms	**451.2960**	**451.2960**	**451.2960**	**451.2960**
WormsTwoClass	78.5920	78.4135	78.7172	**78.3617**
Count	20	19	17	21

The Use of Large Language Models

Large Language Models (LLMs) were employed for proofreading and typographical error correction in this study.